Radargrammetric surface models from Radarsat-2 in Indonesia: Processing and application in tropical forest monitoring

Radargrammetriske overflatemodeller fra Radarsat-2 i Indonesia: Prosessering og anvendelse i tropisk skogovervåkning

Tor Peder Lohne

Norwegian University of Life Sciences
Department of ecology and natural resource management
Master Thesis 30 credits 2012

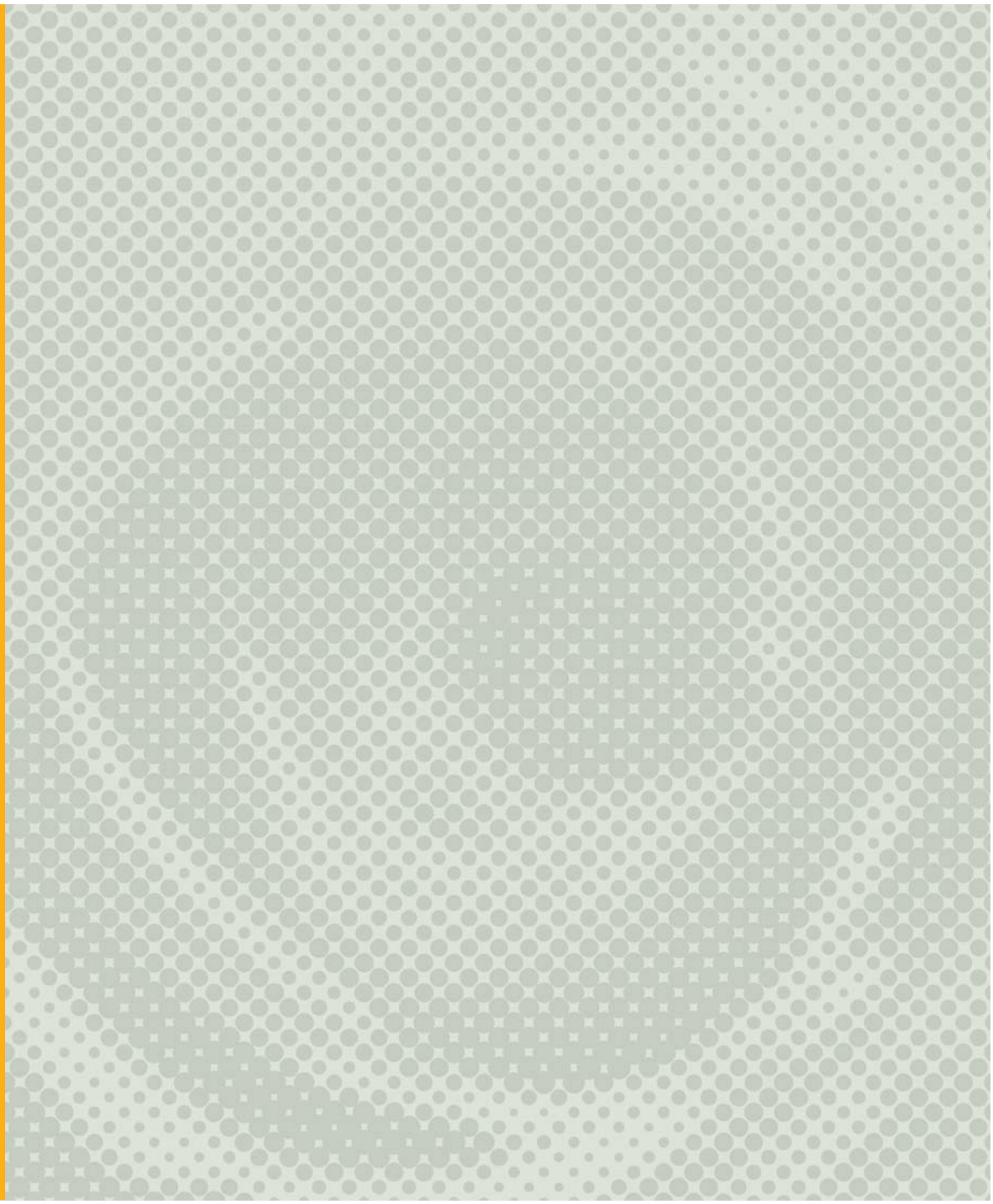

Preface

With this thesis submitted, I have fulfilled my Master of Science degree in Forestry at the Department of Ecology and Natural Resources Management (INA) at the Norwegian University of Life Sciences (UMB).

I would like to thank *Prof. Dr. Svein Solberg*, senior scientist at Norwegian Forest and Landscape Institute (NFLI) and professor at UMB for his patience in supervising my work, sharing from his broad experience in remote sensing and forestry research and thus providing invaluable inputs for my thesis. I would also like to underline my appreciation to *Dr. Dan Johan Weydahl*, senior scientist at the Norwegian Defence Research Establishment (FFI) for co-supervising me and helping me out with SAR and software related challenges.

Great thanks to *Mr. Oka Karyanto* at the Universitas Gadjah Mada (UGM) in Yogyakarta, for being a good cooperation partner in Indonesia. Thanks to *Ismail* for coordination of my field work in Central Kalimantan, for providing me a lot of valuable data and for many interesting discussions. Also, thanks to the rest of the field team from UGM, for bringing and operating the GNSS equipment during the field survey. Thanks to *Mr. Susilo Purnomo*, *Mr. Kasmujiono* and the rest of the staff at Sari Bumi Kusuma (SBK) for supporting my field work in the rainforests of Central Kalimantan. Also, thanks to NFLI and UGM for funding the travel to Indonesia and the field work in Central Kalimantan.

Dr. Janka Dibdiakova and *Johannes Rahlf* at NFLI and *Dr. Ole Martin Bollandsås* at UMB provided general guidance during the study, thank you. I also want to thank *Mrs. Åshild Lysaker* at Geodata AS for supporting me on GIS related inquiries, as well as *Ms. Rut Gallmeier* and *Mr. Stephen Foster* at BAE Systems Inc. for supporting me on Socet GXP.

Last but not least, great thanks to my family, to my dear *Helene* and our beloved son *Ola* for patiently letting me stay at school for late hours during the work on my thesis.

SAR data were provided by Norwegian Space Centre/Kongsberg Satellite Services under the Norwegian-Canadian Radarsat agreement 2011 and 2012.

Ås, December 14th, 2012

Tor Peder Lohne

Abstract

Deforestation and forest degradation contribute to around one fifth of all greenhouse gas emmissions. Hence, measurement, reporting and verification of changes in forest biomass are important in order to help mitigating climate change. Satellite remote sensing in general, and spaceborne Synthetic Aperture Radars in particular, are well suited for tropical forest monitoring, due to the ability to work in areas under persistent cloud cover, typical for tropical forests.

Radargrammetric processing is a possible approach for generating Digital Surface Models from SAR image pairs. The utilization of Digital Surface Models in combination with available Digital Terrain Models may provide Canopy Height Models that may be used to estimate forest biomass. In addition, repeated use of Digital Surface Models may be utilized in order to study the temporal changes in height values. These changes will correspond to the changes of biomass in a given area.

The outline of this study encompassed two challenges related to radargrammetric surface models; the processing of such models in a tropical forest environment in general, and the feasibility of the processed radargrammetric surface models for forest monitoring applications. 18 Radarsat-2 Ultrafine images were utilized for this purpose.

The results showed that image pairs from descending orbits with mean incidence angles of 47.9 and 36.2 degrees generated the best Digital Surface Models. By dividing the amount of biomass in five sample plots with the corresponding Canopy Height Models, a detected increase of 1 meter canopy height corresponded to between 4 and 45 t/ha increase biomass. Partial logging, both strip-logging and selective logging could be detected as change in repeated radargrammetric Digital Surface Models, and the relationship between reported logging quantities and the decrease in Digital Surface Model heights in the corresponding time interval was plausible.

Sammendrag

Avskoging og degradering av skog bidrar til om lag en femtedel av alle klimagassutslipp. Derfor er måling, rapportering og verifisering av endinger i skoglig biomasse viktig for å bidra til å motvirke klimaforandringer. Satellittfjernmåling generelt og satellittbårne Synthetic Aperture Radar spesielt, er velegnet til tropisk skogovervåkning på grunn av evnen til å virke i områder under konstant skydekke, typisk for tropiske skoger.

Radargrammetrisk prosessering er en mulig framgangsmåte for å generere digitale overflatemodeller fra SAR-bildepar. Utnyttelse av digitale overflatemodeller i kombinasjon med tilgjengelige digitale terrengmodeller kan fremskaffe kronehøydemodeller som kan benyttes for å estimere skoglig biomasse. I tillegg kan gjentatt bruk av digitale overflatemodeller utnyttes for å studere temporale endringer i høydeverdier. Disse endringene vil korrespondere med endringer i biomasse i et gitt område.

Denne oppgaven omfattet to problemstillinger knyttet til radargrammetriske overflatemodeller; prosessering av slike modeller i et tropisk skogmiljø generelt, og anvendbarheten av radargrammetriske overflatemodeller for tropisk skogovervåkning. 18 Radarsat-2 Ultrafine bilder ble benyttet til dette formålet.

Resultatene viste at bildepar fra synkende baner med gjennomsnittlige innfallsvinkler på 47.9 og 36.2 grader genererte de beste digitale overflatemodellene. Ved å dividere mengden av biomasse i fem forsøksfelt med korresponderende kronehøydemodeller, fant man at en økning på 1 meter kronehøyde tilsvarte en biomasseøkning på mellom 4 og 45 tonn per hektar. Delvis hogst, både stripe-hogst og selektiv hogst kunne detekteres som endringer i gjentatte digitale overflatemodeller, og sammenhengen mellom rapporterte hogskvanta og reduksjonen i overflatehøyde var plausibel.

List of acronyms

ATPM	*Adaptive Tie Point Matcher*, automatic image matching module in Socet GXP
CHM	*Canopy Height Model*, digital representation of the tree heights CHM = DSM – DTM
DBH	*Diameter at Breast Height*, refers to the diameter of a tree, measured 1.3 meters above the ground (breast height)
DEM	*Digital Elevation Model*, general term for digital representation of elevation and includes both DSM and DTM
DSM	*Digital Surface Model*, digital representation of the surface (e.g. including buildings, vegetation, etc)
DTM	*Digital Terrain Model*, digital representation of the terrain (e.g. bare earth)
GCP	*Ground Control Point*, recognizable point in image, with known coordinates (XY and/or Z)
GHG	*Green House Gases*, including but not limited to Carbon dioxide (CO_2)
GIS	*Geographic Information System*, software for representation and analysis of spatial (geographical) data
GNSS	*Global Navigation System Services*, general term for satellite navigation systems, including but not limited to GPS
GPS	*Global Positioning System*, U.S. satellite navigation system
GDEM	*Global Digital Elevation Model*, digital representation of elevation
GXP	*Geospatial eXploitation Products*, software package from BAE Systems Inc.
ICP	*Independent Check Point*, point with known coordinates, used for accuracy check of DEMs
InSAR	*Interferometric Synthetic Aperure Radar*, SAR applying phase information in the backscatter signal to calculate elevation

IPM	*Interactive Point Measuring*, semi-automatic image matching method in Socet GXP, where the operator is identifying tie points
KSAT	*Kongsberg Satellite Services*, Norwegian satellite data provider
LiDAR	*Light Detection And Ranging*
LOA	*Logged-Over Area*, secondary forests
MRV	*Measurement, Reporting and Verification*, framework for forest monitoring within UN-REDD
NASA	*National Aeronautics and Space Administration*
NGA	*National Geospatial-Intelligence Agency*
NGATE	*Next Generation Automatic Terrain Extraction*, module for DEM generation in Socet GXP
RADAR	*Radio Detection And Ranging*
REDD	*Reducing Emissions from Deforestation and forest Degradation*, framework for mitigation of emissions with application of forest management
SAR	*Synthetic Aperture Radar*
SBK	*Sari Bumi Kusuma*, Indonesian forest concession company, and name of study area
SGF	*SAR Georeferenced Fine*, Radarsat-2 ground range image format
SLC	*Single Incidence Complex*, Radarsat-2 slant range image format
SRTM	*Shuttle Radar Topography Mission*, SAR instrument onboard the space shuttle
UN	*United Nations*
WGS84	*World Geodetic System 1984*, global system for referencing earth's surface, representing the earth as a «perfect» spheroid

Contents

Preface I

Abstract II

Sammendrag III

List of acronyms IV

1. Introduction 1

1.1 Background 1

1.2 Satellite remote sensing 1

1.3 Synthetic Aperture Radar 1

1.3.1 Interferometric SAR 5

1.3.2 Radargrammetry 5

1.3.3 Elevation extraction with SAR 6

1.4 Radargrammetry in forestry applications 7

1.5 Objectives 9

2. Materials and methods 10

2.1 Field data 10

2.1.1 Study area 10

2.1.2 Sample plots 12

2.1.3 Logging data 15

2.2 SAR data 16

2.2.1 Radarsat-2 16

2.2.2 SAR images 17

2.3 Radargrammetric processing of SAR images 19

2.3.1 Image matching 19

2.3.2 Generation of Digital Surface Models 23

2.4 Applications in tropical forest monitoring 26

2.4.1 Relationship between above-ground biomass and canopy heights 26

2.4.2 Detection of partially logged areas 28
3. Results 31
3.1 Radargrammetric processing of SAR images 31
3.1.1 Image matching 31
3.1.2 Generation of Digital Surface Models 33
3.2 Applications in tropical forest monitoring 37
3.2.1 Relationship between above-ground biomass and canopy heights 37
3.2.2 Detection of partially logged areas 38
4. Discussion 42
4.1 Radargrammetric processing of SAR images 42
4.1.1 Image matching 42
4.1.2 Generation of Digital Surface Models 44
4.2 Applications in tropical forest monitoring 48
4.2.1 Relationship between above-ground biomass and canopy heights 48
4.2.2 Detection of partially logged areas 49
4.3 Recommendations for future studies 51
5. Conclusions 52
References 53

1. Introduction

1.1 Background

Emission of greenhouse gases (GHG) may lead to a considerable increase of global temperatures (McKibben 2007), which in turn may lead to climate change and effects on ecosystems. Deforestation and forest degradation contribute to around one fifth of all GHG emissions (Kindermann et al. 2008) and hence forest management and conservation has increased its relevance in the mitigation of climate change (Canadell & Raupach 2008). However, in order to make decisions on the management, forest inventory data is needed. Conducting traditional field-based inventories are often challenging due to the inaccessibility of vast tropical forests, and hence remote sensing may be an appropriate way of collecting the relevant information (Gibbs et al. 2007).

1.2 Satellite remote sensing

During the last few years, remote sensing has got more attention as new methods have been evolving and remote sensing data is more available. Satellite remote sensing is believed to play an increasing role in the measurement, reporting and verification (MRV) of forest and carbon in compliance with the REDD (Reduced Emissions from Deforestation and forest Degradation) mechanism (Gibbs et al. 2007; Holmgren 2008).

Optical imagery have some constraints when it comes to forest monitoring, as the correlation with above-ground biomass has a tendency to saturate at high pixel-values. Also, the humid forests in tropical areas are under persistent cloud cover, which makes monitoring from optical sensors feasible only for a few days of the year. Hence, active sensors which are able to detect features in spite lacking external illumination sources (e.g. sunlight) as well as the ability to overcome the challenges with persistant cloud cover have proven applicable in monitoring of tropical forests. (Gibbs et al. 2007; Rosenqvist et al. 2003)

1.3 Synthetic Aperture Radar

As the term indicates, Synthetic Aperture Radar (SAR) is a type of sensor which transmits and receives radar pulses. It utilizes the time of the signal from transmit to receive in order to calculate the range between the sensor and the reflecting, or so co called backscattering, object. SAR also takes advantage of the Doppler-effect of the radar echoes generated by the

motion of the satellite. This is the “synthetic aperture”; the movement along a flight track and the effect of several pulses backscattered from the desired object “simulate” an antenna larger than the physical extent.

Optical sensors are dependent upon sunlight for illumination and hence observation of objects. In contrast, SAR-sensors provide the illumination with their own radar beam, comparable to the flash of a camera. Because of this, spaceborne radars are able to operate in darkness and can also “see” through clouds. Table 1. shows the comparison of the properties of LiDAR, optical sensors and SAR.

Table 1. Comparison of the properties of LiDAR, optical sensors and SAR (Anonymous 2008)

	LiDAR	Optical	SAR
Platform used	airborne	airborne/spaceborne	airborne/spaceborne
Illumination source	Own radiation (laser)	Reflected sunlight	Own radiation (radar)
Spectrum range	Infrared	Visible/infrared	Microwave
Acquisition in darkness	Yes	No	Yes
See through clouds	No	No	Yes

The backscatter of the SAR signal, i.e. the received intensity of the pixels in the images will vary dependent on the backscattering surface of the objects within the image. Vegetation, i.e. «volume backscatter» are seen as fairly grey spots in the images, while flat surfaces are black as no or little of the SAR signal is reflected back to the sensor. Man-made structures will generate very bright pixels, so called double-bounce. Mountains will generate bright pixels in the slopes facing the sensor, while the back-slopes will be more shadowy. These effects known as «layover» and «shadowing», respectively, are inherent properties of SAR images and can be utilized in classification of the images as well as pattern recognition in image matching processes (Freeman 1996). Figure 1. demonstrates the properties of backscattering surfaces.

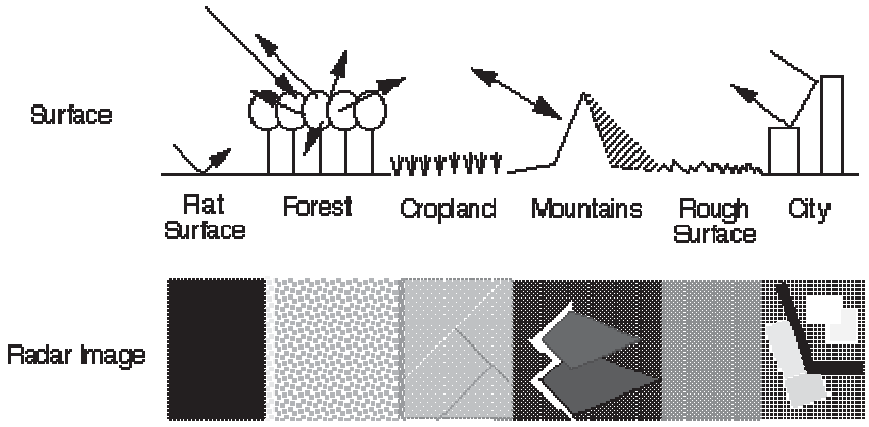

Figure 1. Backscattering properties in SAR images from various surfaces (Freeman 1996)

SAR sensors can acquire images in different modes, namely; *Stripmap*, *ScanSAR* and *Spotlight*. In Stripmap mode, the sensor transmits and receives signals in a constant swath width along its flight track (Figure 1, left). The features within the swath width will be illuminated several times by the pulsed radar transmitter as the motion of the sensor makes overlapping "footprints", thus providing good spatial resolution.

In ScanSAR mode, the sensor takes advantage of the ability to direct the radar beam in multiple incidence-angles, and scans through a number of so-called sub-swaths within the total potential swath width. The benefit is the possibility to detect features in a wider area, however the spatial resolution decrease in this mode as the features will be illuminated less due to the movement of the radar beam in range direction, e.g. the direction perpendicular to the line of flight.

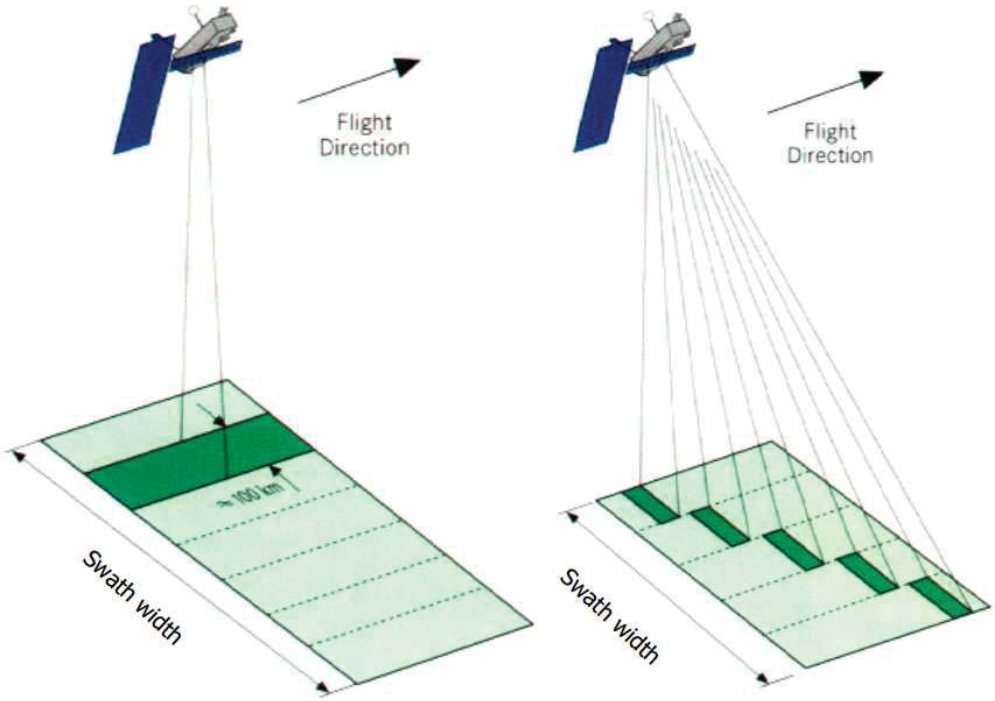

Figure 2. Stripmap (left) and ScanSAR (right) acquisition modes of a SAR sensor (Anonymous 2008)

The spatial resolution of a spaceborne SAR-sensor can be further improved by taking advantage of the Spotlight mode (Figure 3.). With this mode, the SAR-antenna rotates slightly while the satellite flies over a certain area, in order to illuminate the target from even more perspectives than possible in Stripmap mode, thus generating more information about a backscattering object and hence increasing the spatial resolution (Anonymous 2008).

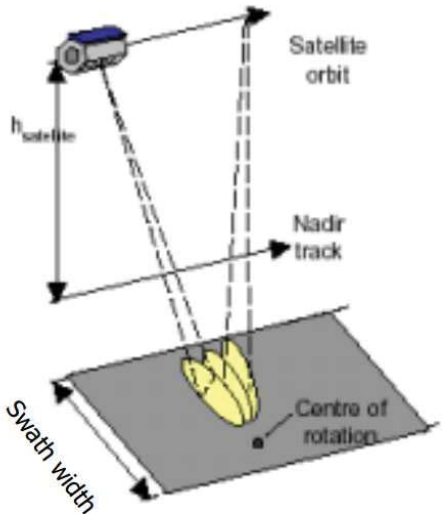

Figure 3. SAR acquisition in Spotlight mode (Anonymous 2008)

1.3.1 Interferometric SAR

Interferometric SAR (InSAR), combines images acquired either by two sensors at different positions simultaneously, so-called single-pass interferometry, or with the same sensor at two different times, namely repeat-pass interferometry. In either case, the system utilizes the difference in the phase of the received signal to measure the range and hence elevations inside the area of acquisition (Toutin & Gray 2000). Because of the temporal decorrelation between images acquired with repeat-pass interferometry over forested areas, i.e. the forest is not exactly the same due to wind, forest management, etc., single-pass interferometry is better suited for extraction of DEMs over forested areas (Balzter 2001).

1.3.2 Radargrammetry

Equivalent to photogrammetry, radargrammetric processing of SAR images exploit the difference in incidence angle in a matched pair of images, combined with the known positions of the sensor in order to calculate the heights of the features being observed by means of trigonometry (Toutin & Gray 2000).

As the positions and orientations of the SAR sensors are known from the onboard GPS, so are the incidence angles. The incidence angles are described as the angle between the line of sight and the line perpendicular to the earth ellipsoid (Fayard et al. 2007). The difference in incidence angle (intersection angle) between to SAR sensors will cause a point (observed in the image acquired from sensor A to move a distance in range direction as observed in the image acquired from sensor B. This distance, also known as the parallax, is proportional to the height of the observed point.

Hence, the intersection angle will determine the heights in the image pair based on trigonometric calculations, as the intersection angles are known throughout the images (Fayard et al. 2007; Toutin & Gray 2000).

The incidence angles provided in SAR sensors suitable for radargrammetry comprise both shallow and steep incidence angles (Figure 4.), e.g. they may vary approximately from 20° (shallow angles) to 50° (shallow angles) (Toutin & Gray 2000). In order to obtain good geometry for height calculation for parallax calculation, the intersection angle between the two images should be large (e.g. one image with shallow incidence angle and one with steep incidence angle). Paradoxically, in order to get as similar images as possible, the images

should have as small intersection angle possible. The latter is an advantage when matching the images, e.g. designating a point in one image to a point in the other image. Hence, a compromise has to be done when choosing acquisition parameters; large intersection angles for good geometry versus small intersection angles for good image matching. The matching of the images is a fundamental of the radargrammetric image processing (Toutin & Gray 2000).

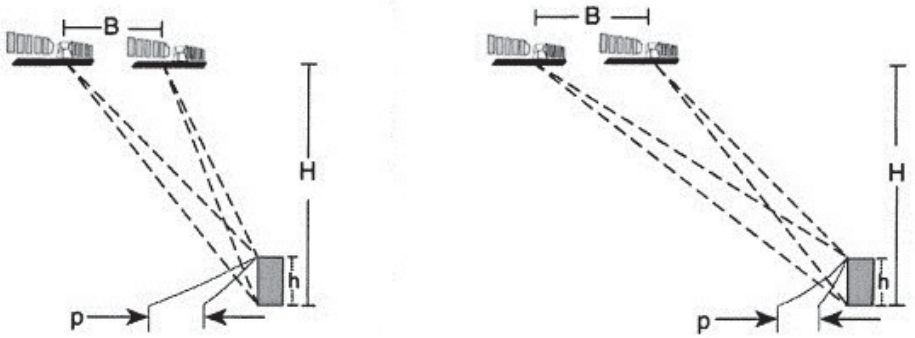

Figure 4. The principle of radargrammetry Steep (small) incidence angles (left) and shallow (large) incidence angles (right) (Toutin & Gray 2000)

1.3.3 Elevation extraction with SAR

SAR data may be used to derive three-dimensional information, by combining multiple SAR images in various methods covered by the term «3D-SAR», including, but not limited to Interferometric SAR (InSAR) and radargrammetry.

While interferometry is considered the most accurate method for elevation extraction, the potential of radargrammetry lies in the availability of sensors, in contradiction to InSAR which is only feasible with certain sensors. This is particular for forest applications, as single-pass acquisitions is the preferred technique in interferometry due to the temporal decorrelation of repeat-pass interferometry (Balzter 2001).

Canopy height is an important parameter in forest monitoring, owing to the strong correlation with forest biomass (Solberg et al. 2010). A Canopy Height Model (CHM) can be extracted by subtracting an existing Digital Terrain Model (DTM) from a Digital Surface Model (DSM) derived from 3D SAR; CHM = DSM – DTM (Figure 4.).

However, one disadvantage of this method is that DTMs are often hard to obtain in remote forest areas (Perko et al. 2011).

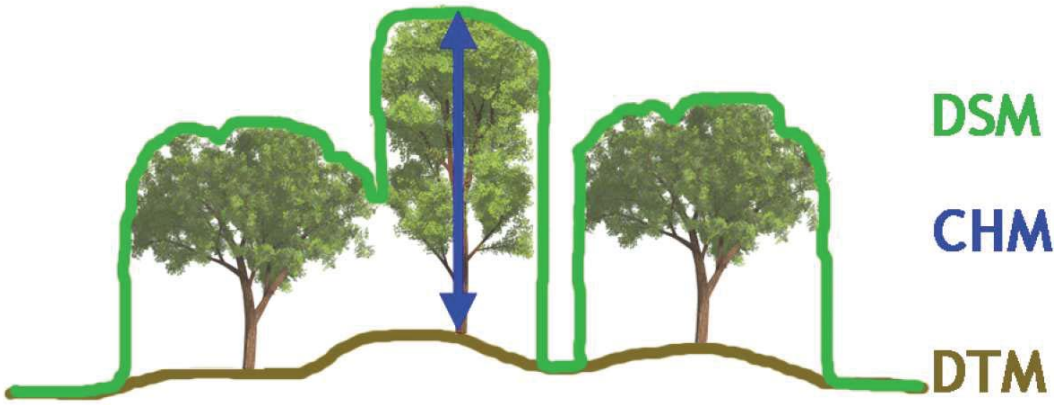

Figure 5 Explanation of Digital Surface Model (DSM), Digital Terrain Model (DTM) and Canopy Height Model (CHM). CHM = DSM – DTM (Perko et al. 2011)

1.4 Radargrammetry in forestry applications

Extraction of forest canopy height has proven important, as the correlation between the "raw" intensity properties, i.e. brightness of pixels in SAR images, and forest biomass saturates at fairly low levels of biomass (Gama et al. 2010; Neef et al. 2005).

It should be noted that tree heights are underestimated with SAR due to a penetration of the radar signal into the forest canopy caused by the wavelength of the signal. Regardless of this, the forest structure has to be taken into account, as the radar heights are dependent on a combination of tree heights and forest density. Hence, the CHM from SAR images is believed to be better correlated with above-ground biomass than tree heights (Solberg et al. 2010).

Previous studies demonstrated the applicability of radargrammetric surface models in forest applications. Plot-level forest variables were predicted in a Finnish forest applying radargrammetry on images acquired with TerraSAR-X. They were able to predict stem volumes up to 400 m^3/ha with a relative error (RMSE %) of 34 % for a test plot with size less than 0.1 ha (15 m radius). There was no clear indication of a saturation level in the stem volume estimation (Karjalainen et al. 2012).

One study applied radargrammetric surface models processed with images from the TerraSAR-X and COSMO-SkyMed satellites, to extract canopy height models (CHMs) from two test sites in Austria. Combining CHMs with X-band backscatter information and interferometric coherence, they were able to classify forest regions with an accuracy of 90 %.

They found a standard deviation height error less than 2 meters over forests (Perko et al. 2011).

Assessments of radargrammetric DSMs from TerraSAR-X stripmap images in a mountainous area of the Amazon, found that root mean square errors (RMSE) less than 6.67 meters could be obtained, utilizing a minimum of 8 ground control points (GCPs) (De Oliveira et al. 2011).

In an operational forest monitoring system the ability to detect and quantify changes in the biomass stocks may be important in order to determine whether the forest management is in compliance with the stated intentions. Especially, the ability to detect partial logging may prove important, due to the fact that much of this type of logging is due to illegal activity (Fuller 2006).

Former studies demonstrated the applicability of radargrammetry for calculation of absolute values of forest biomass. However, there is also a greater potential in the application, namely the utilization of repeated radargrammetric surface models for detection of changes in forest biomass. Owing to the higher availability of radargrammetric SAR acquisition (in contrast to interferometry) combined with unexplored potential of radargrammetry in change detection – this is what I wanted to examine in my study.

1.5 Objectives

The outline of this study encompassed two challenges related to radargrammetric surface models; the processing of such models in a tropical forest environment in general, and the feasibility of the processed radargrammetric surface models for forest monitoring applications. These challenges were specified in three objectives. I wanted to:

a) determine which Radarsat-2 acquisition properties give the best Digital Surface Models (DSM) in a tropical forest environment

b) extract Canopy Height Models (CHM) by subtracting terrain height values from the surface height values, and describe the relationship between the CHM height and above-ground biomass

c) determine whether partial logging can be detected as changes in repeated radargrammetric DSMs.

2. Materials and methods

This study is characterized by its pioneer work, with the application of methods that are not widely demonstrated before. Results from studies utilizing radargrammetric DSMs for biomass change detection and quantification has not been published previously.

Technical, cultural and lingual challenges made the task difficult, and the data sets were not as comprehensive and good as planned, in terms of number of sample plots and uncertainty in location accuracy. Still, I believe the data was sufficient for conducting a valuable study.

2.1 Field data

The field data were in general characterized by uncertainty and thus some limitations arose. Initial plans involved the utilization of a larger number of well-distributed sample plots, in order to study the correlation between measured above-ground biomass and extracted CHMs.

I teamed with four students and one coordinator from the Universitas Gadjah Mada (UGM) in Yogyakarta in late October 2011. Together we conducted a field survey, measuring the intended sample plots. However, misunderstandings led to satellite acquisitions some kilometers north-east of the intended study area, and hence the measured plots could not be used. Thus, a second field survey was conducted for the plots that were covered by the Radarsat-2 acquisitions, this time without me participating.

2.1.1 Study area

The area of interest, “SBK”, is a tropical forest area in Central Kalimantan on Borneo in Indonesia, just south of the equator line and 330 km east-southeast from the west-coast city Pontianak (Figure 6.). Geographical coordinates -0.7N 112.2E.

The topography comprises lowlands in the center of the area while the eastern and western parts comprise high relief terrain, i.e. mountainous areas. Elevation ranges approximately from 200 meters in the center of the area to 1200 meters above mean sea level in the mountains surrounding the lowlands. The majority of the area ranges from 200 meters to 300 meters above sea level. The weather conditions in the area are characterized generally by high temperatures and humid air. Heavy rain showers may occur suddenly during the entire year, and the rainy season with the most precipitation lasts approximately from November to May. Detailed weather records from the SAR image acquisitions are presented in Table 2.

The study area is part of a concession forest currently held by *Pt. Sari Bumi Kusuma* (SBK), an Indonesian forestry company and a part of *Alas Kusuma Group*, one of Indonesia's major industrial groups. In the following, SBK refers to both the name of the company and the designation of the study area. The size of the concession area was 147.600 ha (Figure 6, right), and it consists of both virgin and secondary forests stands, the latter called *Logged-Over Areas* (LOA). For this study area, stands can be regarded management units, e.g. the overall plans for logging and planting activity consider one stand as a single unit. Typical size of forest stands vary approximately from 10 to 100 hectares.

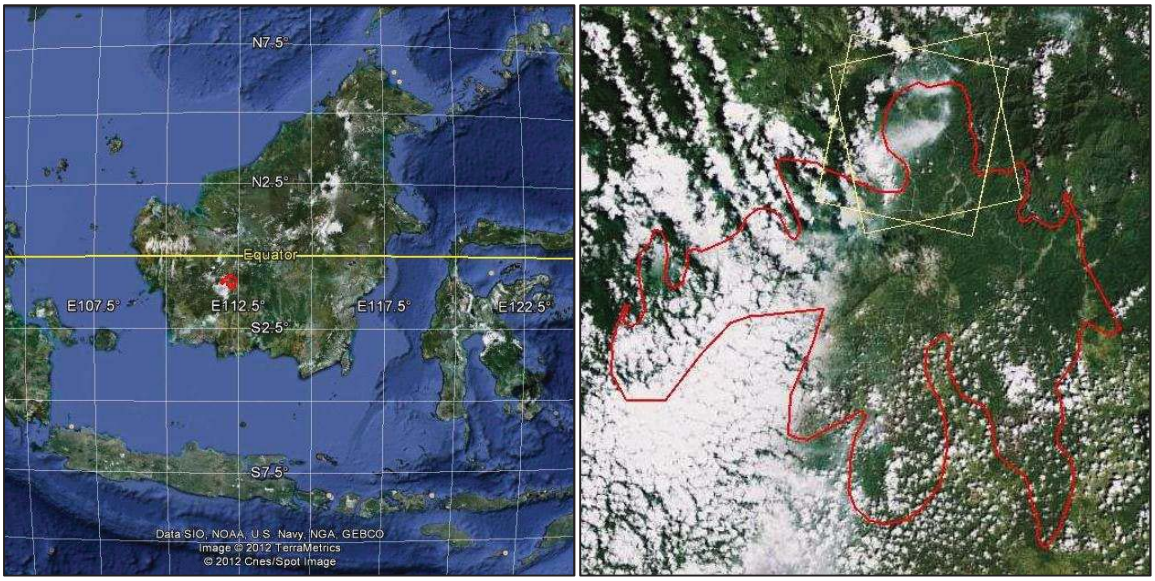

Figure 6. Map over Borneo with the study area "SBK" in red color (left), and the concession area in red with Radarsat-2 coverage area marked with yellow squares, measuring approximately 20x20 km. Image courtesy of Google Earth 2012.

SBK perform year-round forest operations, and though it is hard to get historical data from the logging operations, reports indicate an annual logging volume of approximately 120.000 m^3 in 2011. Logging volumes are regulated in the concession from the Indonesian government (Kasmujiono 2011).

Numerous tree species exist in SBK, with *Dipterocarpaceae spp*. as the most common family with more than two-thousand unique species. SBK applies two silviculture systems; namely strip logging and selective logging. The former is selective logging (Figure 7.) of trees above 40 cm DBH (diameter at breast height) in 3 meter wide strips with 17 meter intact forest between the strips. The latter is selective logging of trees above 50 cm DBH. In either case 23 commercial species are legally logged, from which 15 are *Dipterocarpaceae spp*. Fruit-

bearing trees are prohibited from logging as they provide food for wild animals. Although the logging is selective, unintentional damage and even intentional logging of trees surrounding the commercial species may occur, often unavoidable due to the dense structures in tropical forests. Indeed, strip-logged areas are as a matter of fact clear-cut.

Both strip-logging as well as selective logging may be applied in virgin- as well as secondary forest compartments. Areas with slopes from 0 to 25 % are managed as strip-logging areas, while selective logging is applied in areas with slopes between 26 and 40 %. This is mainly due to the constraints of the logging equipment. Areas with slopes above 40 % are restricted for conservation (Kasmujiono 2011).

Figure 7. Aerial photo of a strip-logged stand. The logged strips are 3 meters wide and the spacing between the strips is 17 meters (Ismail 2012).

2.1.2 Sample plots

Because of a misunderstanding, SAR image acquisitions were ordered for an area that did not comprise a large number of sample plots, in contradiction to the intention. However, new possibilities emerged, as the selected area of image acquisitions covered stands being logged in 2011. Hence, this made it possible to study the potential of change detection with repeated use of radargrammetric DSMs.

The field data consisted of 5 square-shaped sample plots, i.e. 6CC, 6DD, 7Q, 7R and 7V (Figure 8.). The sample plots were of 1 ha size, and had undergone an inventory in 2008. Every single tree within each sample plot was measured by means of diameter at breast height (DBH) as well location (easting and northing) of all trees from 10cm DBH and above. Trees were manually located with measuring tape and compass, with positions relative to the plot corners (Kasmujiono 2011). In addition to vegetation data, digitalized contour lines were provided separately for all plots, enabling the making of DTMs for each sample plot.

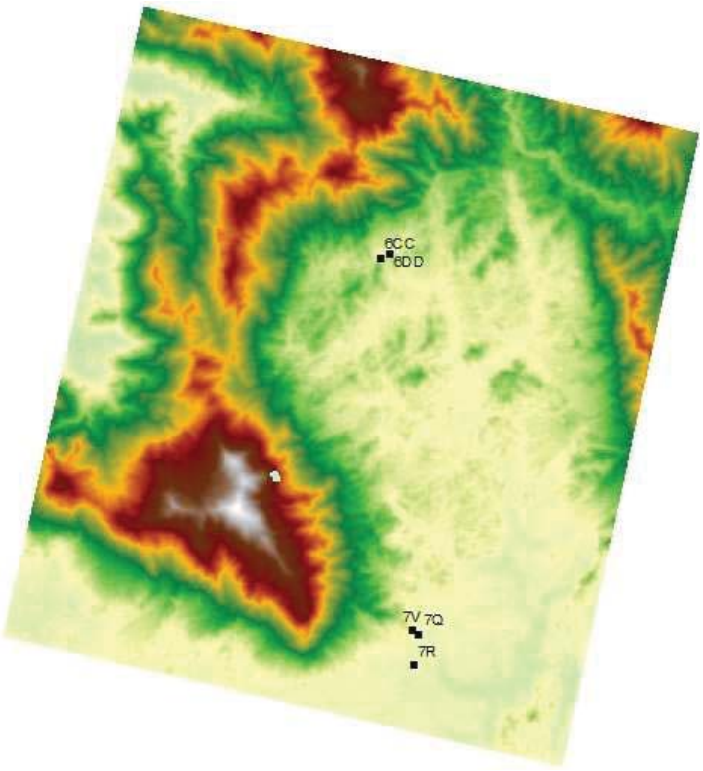

Figure 8. The locations of the sample plots 6CC and 6DD in north of the study area, and 7Q, 7R and 7V in south.

The relative location accuracy within the sample plots were deemed sufficient. However, in order to utilize the terrain data, the absolute location accuracy had to be improved. For this purpose I joined a field survey conducted in the last two weeks of October 2011. The objective of the survey was to accurately locate the sample plots by measuring XYZ-coordinates in one corner of each plot within the Radarsat-2 coverage area with differential GPS (dGPS) receivers.

Figure 9. Work with Topcon Hiper II GNSS-receiver in the road close to one of the sample plots

Due to dense canopy cover inside the sample plots, we had to set up the GNSS (Global Navigation Satellite System) receivers in the road close to each plot (Figure 9.), in order to get sufficient connection with the GNSS-satellites. Two dual-frequency *Topcon Hiper II* receivers (TopCon 2012) were recording positions simultaneously for 1-3 hours, with the aim of getting the highest possible accuracy. One receiver maintained the same position during the survey, in order to take into account possible GPS "drift-off", e.g. relative spatial inaccuracy due to the inherent properties of GPS. In addition, the coordinates were post processed with the utilization of a reference station with known XYZ-coordinates operated by *Bakosurtanal*, the Indonesian mapping authority. All geodetic measurements and calculations were conducted by our Indonesian counterpart (Ismail 2012). As the GNSS receivers were not set up in the plots directly, distance as well as horizontal and vertical angles from the appropriate corner of the plot to the receiver were measured with the use of measuring tape, compass and hypsometer (Figure 10.).

Figure 10. Measurement of inclination with LaserAce hypsometer (Trimble 2012)

2.1.3 Logging data

In conjunction with the study of the ability to detect partially logged areas a dataset consisting stand-wise logging data from 2011 was utilized for validation of detected changes in the DSMs generated from image pairs acquired in different time periods, as explained in chapter 2.2.2.

The dataset provided numbers from 22 forest stands that were logged during 2011 (Figure 11.) including type of logging (strip- or selective logging), area of the stands, time period the stands were logged, as well as number of trees and volume of logged trees.

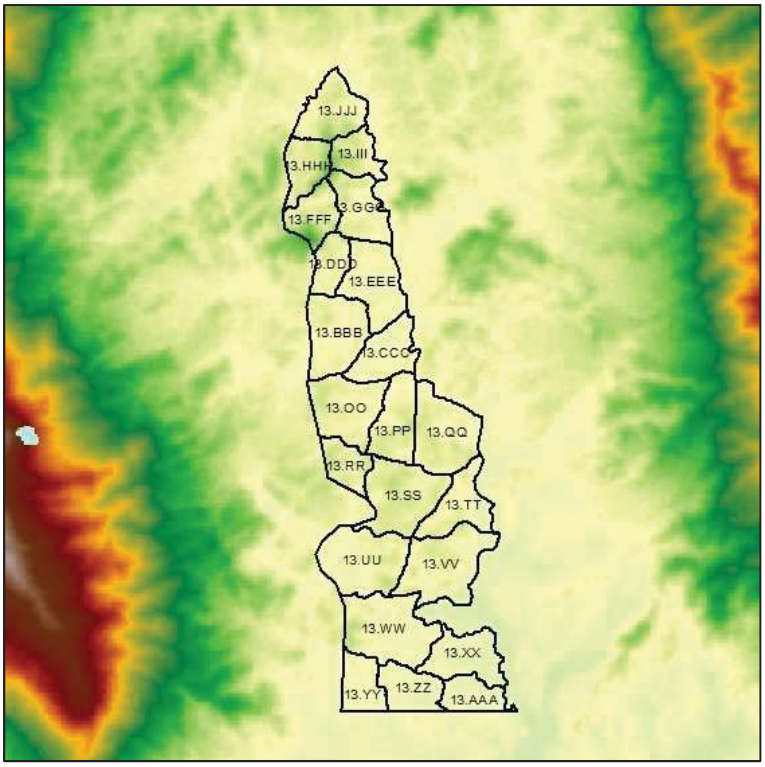

Figure 11. Map of the stands that were prtially logged in 2011

2.2 SAR data

2.2.1 Radarsat-2

Radarsat-2 is a Canadian earth observation satellite with a Synthetic Aperture Radar (SAR) payload on board. It was launched in December 2007 and put into operation the following year. The satellite orbits the earth in an altitude of 798 km, in a sun-synchronous, dusk-dawn orbit i.e. ascending pass in the morning and descending pass in the afternoon (MDA 2007).

The SAR sensor is right-looking, i.e. images acquired in ascending orbits will be illuminated from west, images acquired in descending orbits will be illuminated from east. It operates in C-band, which implies a wavelength of the radar signal of approximately 6 cm. It can acquire images in *Stripmap*, *ScanSAR* of *Spotlight* mode, comprising a comprehensive range of sub-modes (Figure 12.) (Slade 2011).

The variety of modes yields wide-area acquisitions or smaller areas with enhanced spatial resolution. Radarsat-2 offers incidence angles varying from 20 to 60 degrees, making the sensor suitable for generation of radargrammetric surface models (Toutin 2010).

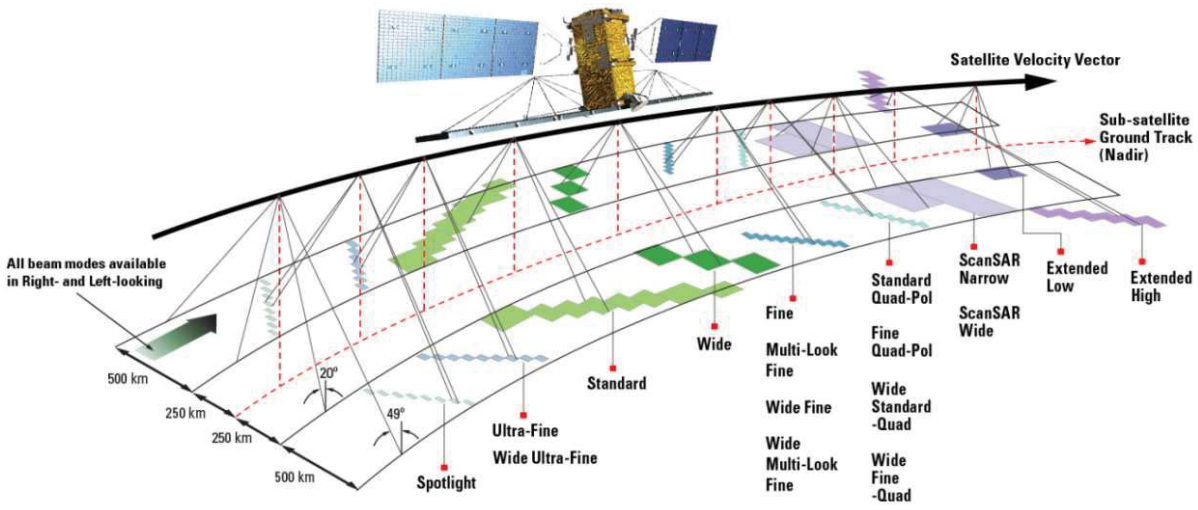

Figure 12. Radarsat-2 with the variety of image acquisition modes (Slade 2011)

2.2.2 SAR images

Eighteen Radarsat-2 images from SBK were utilized for radargrammetric processing. The images were acquired during three time periods; six images were acquired in November 2011, six in May and June 2012, while the last six images were acquired in November 2012 (Table 2.).

The acquisitions were done from the same six orbital planes in all three periods; three descending and three ascending orbits. All images were acquired in *Stripmap* mode and *Ultrafine* resolution, i.e. spatial resolution of 3 meters, with mean incidence angles varying from 21.7 to 47.9 degrees. The SAR images were downloaded and pre-processed into a georeferenced (e.g. all image pixels were assigned to north- and east-coordinates) SGF-format by Kongsberg Satellite Services in Tromsø, and made available through a FTP-server. A sample SAR image is shown in Figure 13.

Table 2. Overview of the Radarsat-2 images acquired in this study. Orbit direction refers to the pass direction of the satellite, either from south towards north (ascending) or from north towards south (descending). Incidence refers to the incidence angle of the image, numbers in degrees. Temperatures and humidity, as well as precipitation were recorded from a weather station in Nanga Pinoh, approximately 60 km north of the study area. Precipitation measured accumulated from previous acquisition except from first acquisition (*) in each time period.

Image Nr	Acquisition Date	Time (UTC)	Orbit direction	Incidence (degrees)	Temp (°C)	Humidity (%)	Precipitation (mm)
01	01/11/2011	22:05:40	Desc	47.9	26	74	4*
02	05/11/2011	10:52:56	Asc	38.5	25	79	40.0
03	11/11/2011	22:13:56	Desc	36.2	27	77	11.5
04	19/11/2011	10:44:39	Asc	24.7	27	78	17.1
05	21/11/2011	22:22:12	Desc	21.7	26	80	0.0
06	22/11/2011	10:57:03	Asc	44.7	29	74	0.5
07	21/05/2012	22:13:57	Desc	36.2	27	78	0.5*
08	29/05/2012	10:44:39	Asc	24.7	26	80	28.0
09	31/05/2012	22:22:12	Desc	21.7	28	68	0.0
10	01/06/2012	10:57:03	Asc	44.7	26	82	0.8
11	04/06/2012	22:05:40	Desc	47.9	28	79	45.0
12	08/06/2012	10:52:56	Asc	38.5	29	69	28.0
13	13/11/2012	10:44:42	Asc	24.7	26	81	89.5*
14	15/11/2012	22:22:14	Desc	21.7	26	84	0.0
15	16/11/2012	10:57:06	Asc	44.7	26	80	0.0
16	19/11/2012	22:05:41	Desc	47.9	29	81	8.0
17	23/11/2012	10:52:57	Asc	38.5	27	78	0.0
18	29/11/2012	22:13:58	Desc	36.2	26	84	18.0

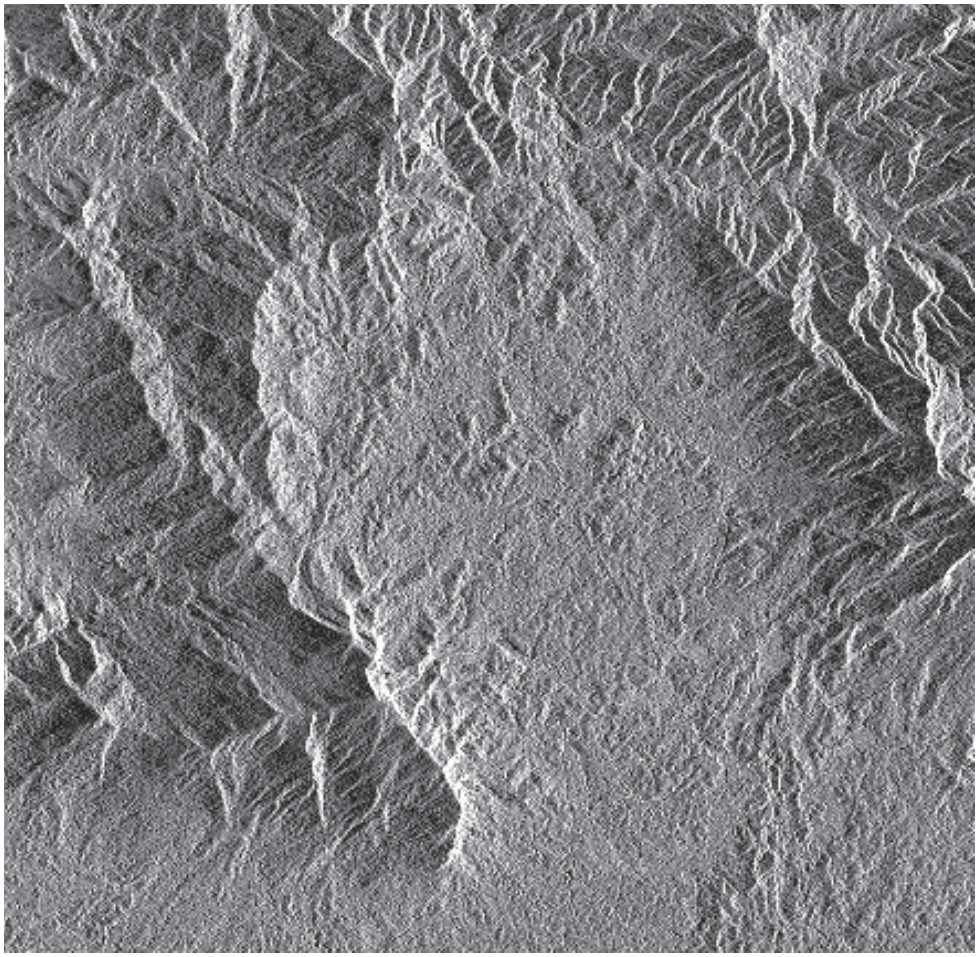

Figure 13 Sample SAR image (#02) from the study area

2.3 Radargrammetric processing of SAR images

The outline of the radargrammetric DSM generation (Figure 14.) consists of matching pairs of SAR images acquired from different incidence angles, where the parallax based on the difference in incidence angle in the two images are being used for height computation (Toutin & Gray 2000).

Then, a Digital Elevation Model (DEM) can be generated, based on the resulting image match. All this can be done in commercial photogrammetric software. I used the Socet GXP software (BAE 2012).

The SAR images had orbital- and orientation data provided in supplementary header files, which can be utilized in Socet GXP.

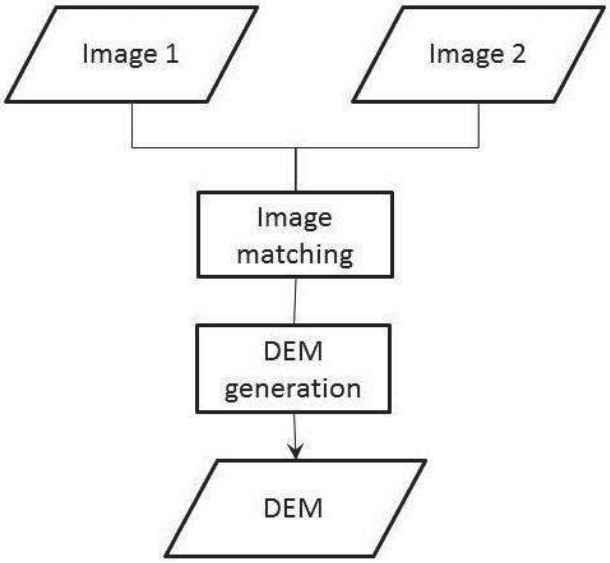

Figure 14. Simplified sketch of the process from an image pair to the digital elevation model

2.3.1 Image matching

The purpose of the image matching process is to tie the two images together by finding corresponding tie points in the images, in order to make the basis for the generation of the digital elevation models. Two different strategies in performing the image matching were carried out in Socet GXP; semi-automatically with the so-called *Interactive Point Measurement* (IPM) module, where the operator manually identify tie points, or a fully automatic module, namely *Adaptive Tie Point Matcher* (ATPM), where tie points are

identified by the program. In both IPM and ATPM, the program matches the two images, based on the identified tie points. It is performing a search for other corresponding points, i.e. “matched points” around the tie points with some sort of image matching algorithm. The exact properties of this algorithm remain unknown, as this specific documentation was not provided by BAE Systems.

Matched image pairs were evaluated by studying the tie points, i.e. the number of tie points generated as well as their location accuracy.

All image pairs were matched with both IPM and ATPM in order to study if the matching strategies themselves would have any effect on the processed DSMs. Images pairs were formed by same-side SAR images, thus giving 6 image combinations per acquisition period (i.e. November 2011, May/June 2012 and November 2012). Details provided in Table 3.

Semi-automatic image matching

With IPM, the operator is identifying tie points in both images with the human eye. This is a time consuming process, as the properties of SAR images require practice, in order to recognize the corresponding patterns in two images. Corresponding points are most easy found in connection with infrastructure, e.g. man-made structures, because the bright pixels in the images due to «double bounce» from the structures may be utilized. In addition to bright pixels, the shadowing effect of the trees near roads may be utilized. These shadows were more distinct in images with high incidence angle, and hence it was easier to identify tie points manually in these images.

However, differences between the images due to the intersection angle also causes difficulties matching the images, simply because they are not completely similar. Figure 15. demonstrates the difference between images with various incidence angles in both orbit directions.

Automatic image matching

In contradiction to IPM, the program is identifying tie points automatically with ATPM, initially by laying out a systematic grid of tie points, and then searching for corresponding points with these tie points as a basis. The tie points finally identified may however differ slightly from the original grid, dependent on the ability of ATPM to find corresponding points in the two images (Figure 16.).

Table 3. Overview of all image pairs (first coloumn). Orbit direction refers to if the satellite is travelling from south to north (ascending) or from north to south (descending). The intersection angle is the difference in incidence angle between the images in the respective image pair. Interval refers to the time from the first image acquisition to the last

Image pair	Acquisition period	Orbit direction	Intersection (degrees)	Interval (days)
A0204	November 2011	Ascending	13.9	14
A0206	«	Ascending	6.2	17
A0406	«	Ascending	20.1	3
D0103	«	Descending	11.7	10
D0105	«	Descending	26.2	20
D0305	«	Descending	14.5	10
A0810	May/June 2012	Ascending	20.1	3
A0812	«	Ascending	13.9	10
A1012	«	Ascending	6.2	7
D0709	«	Descending	14.5	10
D0711	«	Descending	11.7	14
D0911	«	Descending	26.2	4
A1315	November 2012	Ascending	20.1	3
A1317	«	Ascending	13.9	10
A1517	«	Ascending	6.2	7
D1416	«	Descending	26.2	4
D1418	«	Descending	14.7	14
D1618	«	Descending	11.7	10

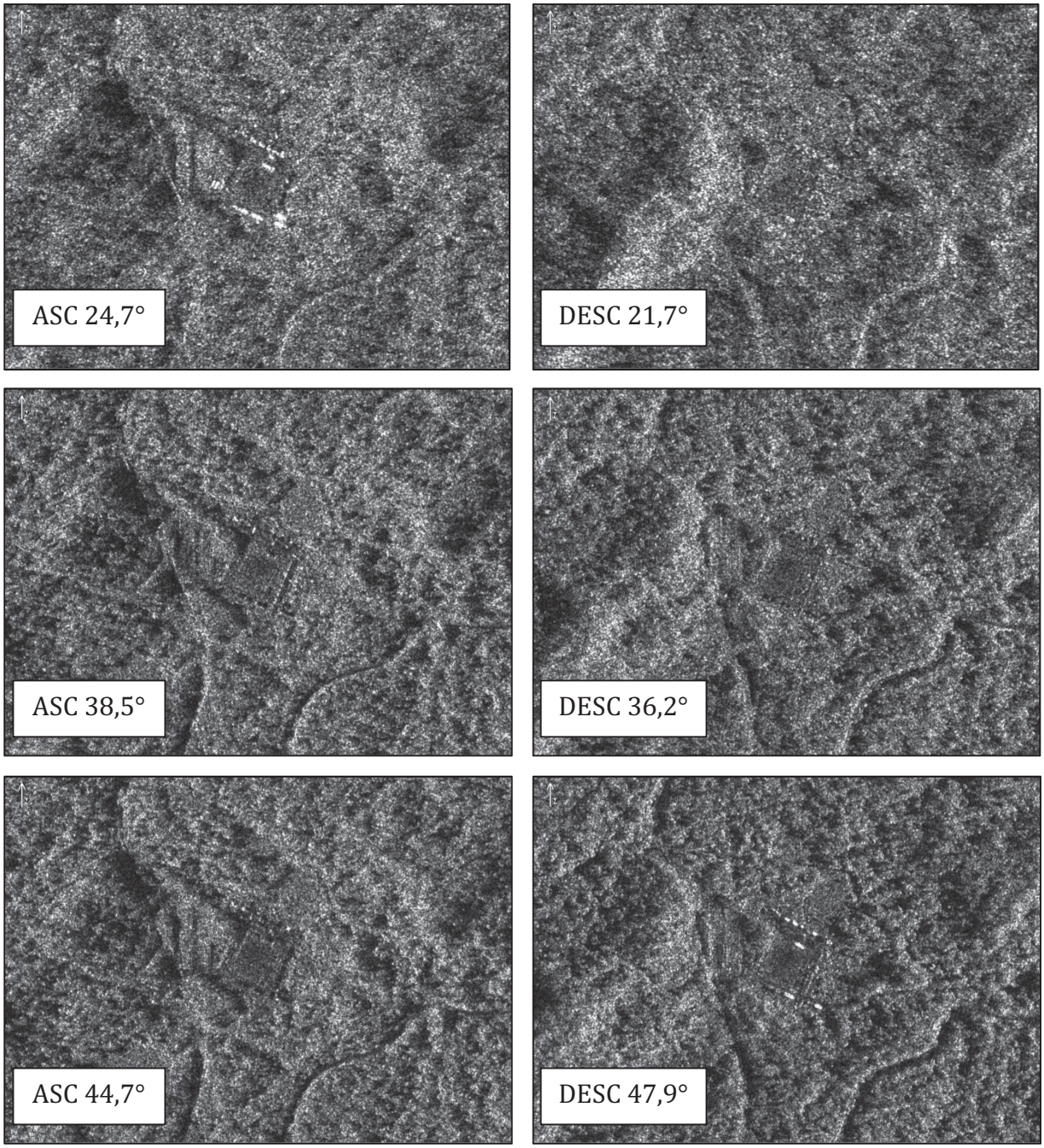

Figure 15. Sample area showing a camp and some roads in the forest. Orbit directions (ascending/descending) and incidence angles specified. Note the difference in brightness of pixels representing buildings in the center of the images. Also note the shadows near the roads, more distinct in images with high incidence angles, and the indistinct features of the image with smallest incidence angle, i.e. 21.7 degrees. Higher incidence angle means closer to horizontal.

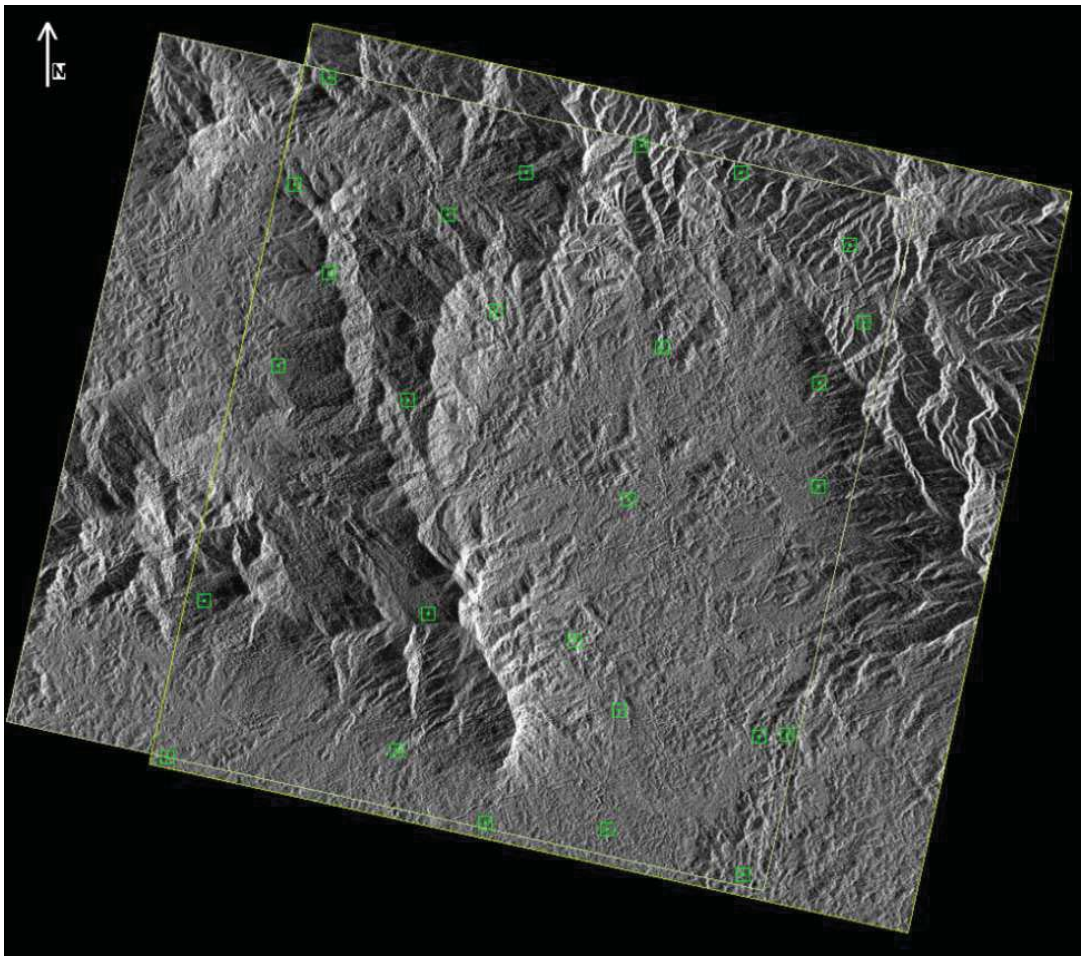

Figure 16. Two SAR images (#01 and #03, forming image pair D0103) with tie points identified by ATPM

2.3.2 Generation of Digital Surface Models

Socet GXPs module used for DSM generation is called *Next Generation Automatic Terrain Extraction* (NGATE). All DSMs were processed to a georeferenced (i.e. all pixels were assigned to a XYZ-coordinates) tif-format (GeoTIFF) with 10 meters pixel spacing, in the WGS84 reference system.

Information about all the digital surface models generated could be found in Table 3. Also note that the corresponding six orbits and thus incidence angles were applied in all three acquisition periods.

Ground Control Point

The image pairs from November 2011 were processed with the use of a single ground control point (GCP). A GCP is used for referencing the SAR images to the ground coordinate system. Thus it should have known XYZ-coordinates and it should be seen as a bright pixel in the SAR image (Figure 17. right). For this purpose, a trihedral corner reflector was set up during the acquisition period in November 2011 (Figure 17. left). The coordinates of the reflector were measured by means of differential GPS during the field survey, and the orientation was adjusted according to the Radarsat-2 acquisition plan, so that it would face the satellite in each image.

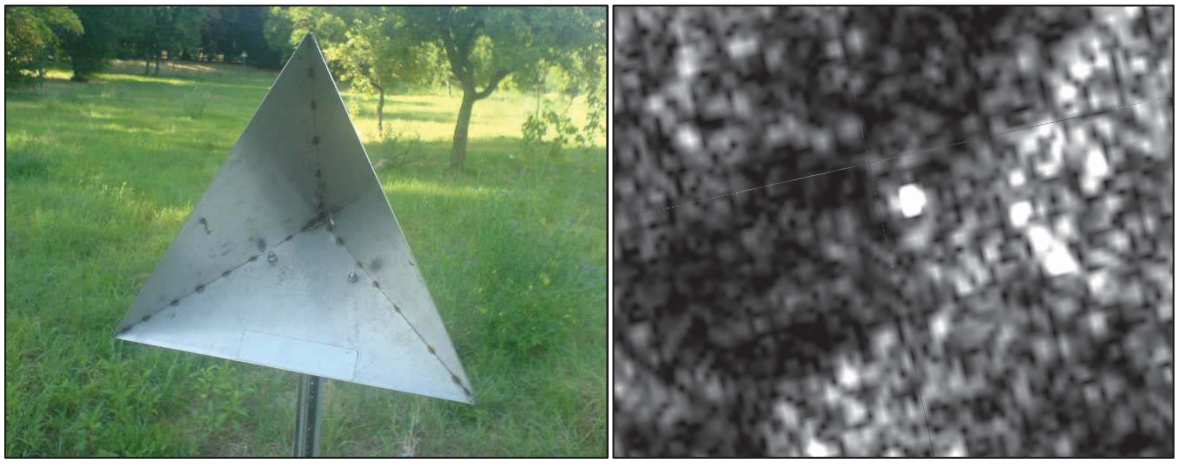

Figure 17. Trihedral corner reflector (left) (Wikipedia 2007) and the reflector seen as a bright point in the center of the image (right)

Regarding the images from May/June 2012 and November 2012, no GCP were utilized as the corner reflector could not be set up. Hence, the images from these acquisition periods could not be processed with the utilization of GCP.

Visual interpretation of the DSMs

Prior to accuracy assessments, the DSMs from each acquisition period, one ascending orbit and one descending orbit were chosen, as evaluated by means of visual interpretation. The visual interpretation was performed by comparing the processed DSMs with a 30x30 meter "reference DSM" (Figure 17.) acquired by the SRTM (X-band InSAR mission) in year 2000. The generated DSMs were simply classified as either "poor" or "good", based on the general

representation of the overall topography, the amount of observed noise and artifacts, the level of details shown, and finally the similarity with the SRTM DSM.

Accuracy assessments

Accuracy assessments of the DSMs were performed by utilizing 8 Independent Check Points (ICPs) (Figure 18.) for calculating difference in height (dZ) values. The ICPs were measured using differential GPS (dGPS) during the field survey, and consisted of XYZ-coordinates measured in the road close to the sample plots as well as other random locations within the coverage area of the SAR images. However, as the points could not be identified in the images, only height accuracies (Z) could be assessed. Thus, the DSMs were considered accurate in terms of planimetry (X and Y), relatively speaking. This means, the planimetric accuracies were assumed sufficient for comparisons between the DSMs. Height deviations (dZ) were expressed as $dZ = Z_{ICP} - Z_{DSM}$. The calculated values included mean height deviation (bias), RMSE and standard deviation of the heights. The ICPs were distributed throughout the lower parts of the area (Figure 18.) at elevations ranging approximately from 171 to 331 meters above mean sea level.

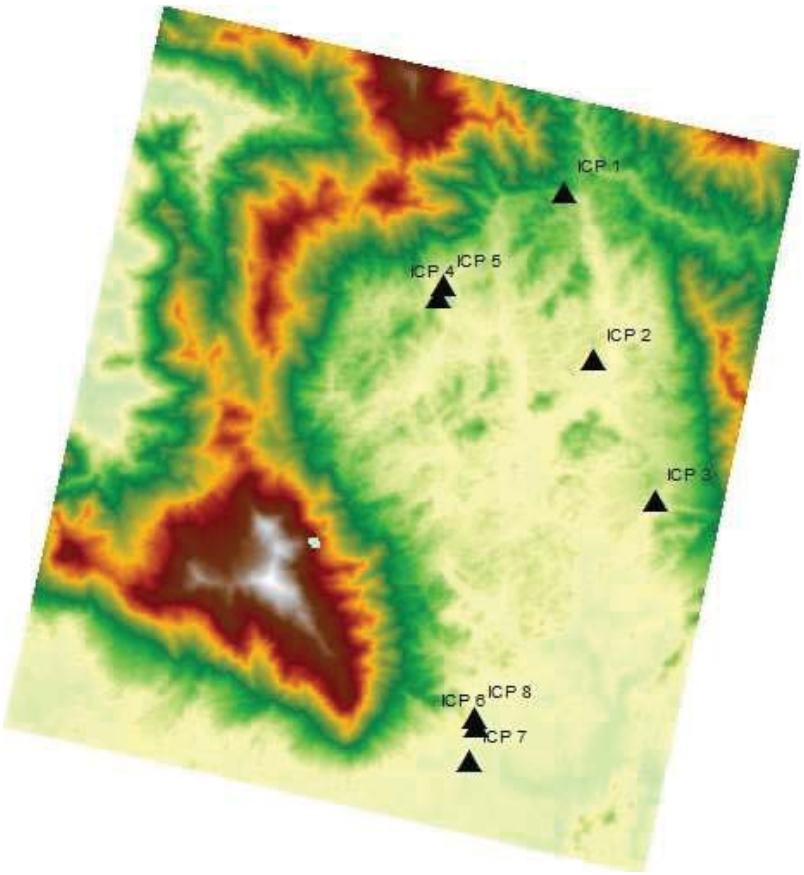

Figure 18. The Independent Check Points (ICP) distribution in the area of interest, laid over the SRTM "reference DEM"

2.4 Applications in tropical forest monitoring

The application of the DSMs for tropical forest monitoring was evaluated with two different approaches. Firstly, the relationship between above-ground biomass and canopy heights was evaluated, by dividing the amount of biomass in each plot with the corresponding canopy height model (CHM) extracted from all image pairs.

Secondly, repeated DSMs generated from image pairs acquired in different time periods were utilized, in order to study the change of DSM heights over partially logged stands. Changes in DSM heights were validated using stand-wise logging volumes as "ground truth", displayed in a map with graduated colors representing the averaged logging volumes per stand. Finally, the detected stand-wise mean values of DSM height changes were used to predict the logging volumes with simple linear regression analysis.

2.4.1 Relationship between above-ground biomass and canopy heights

Above-ground biomass was calculated with an allometric function developed for SBK specifically. The biomass was calculated per sample plot with the sum of biomass for all measured trees (Equation 1.) (Karyanto 2011). However, the measured trees did not include the total amount of biomass, and based on my own experience from the actual study area, assumptions were made that the calculated biomass included approximately 75 % of the actual above-ground biomass.

Equation 1:

$$Biomass = (0.0505 * (Dbh^2 * H)^{0.9464}) - (0.0101 * (Dbh^2 * H)^{0.8861})$$

DBH = diameter at breast height
H = tree height calculated from Equation 2.

Biomass calculated for all trees were accumulated per sample plot.

As the tree heights were not measured, height values were estimated with the use of another allometric function. DBH given in centimeters provided heights given in meters (Equation 2.).
Equation 2:

$$H = \frac{1}{0.3536 * \left(\frac{1}{DBH}\right) + 0.028}$$

It has been demonstrated that allometric biomass calculations without height as input can be almost equally accurate than calculations with height as input (Basuki et al. 2009). Hence, I believe that the lack of height measurements was of minimal importance to the biomass estimations. Calculated above-ground biomass in the various sample plots based on the inventory data and the allometric equations (Equations 1. and Equation 2.) ranged from 145 to 312 tons per hectare (Table 4.)

Table 4. Calculated above-ground biomass in sample plots, values in tons per hectare (t/ha)

Plot	6CC	6DD	7Q	7R	7V
t/ha	225	201	221	145	312

With the utilization of the contour lines (mentioned in chapter 2.1.1), local digital terrain models were extracted for each sample plot. The DTMs were then positioned according to the XYZ-coordinates measured during the field survey.

One of the sample plots, 6CC had for some reasons no measured coordinates. Hence, this plot retained its «original» coordinates, which accuracy may be considered highly uncertain, as the native method of locating the sample plots was unknown, but possible with the use of hand-held navigational GPS devices.

Canopy Height Models (CHMs) were created for each sample plot, by subtracting the Digital Terrain Models (DTMs) from the various radargrammetric Digital Surface Models (DSMs) (CHM = DSM – DTM), using the *Raster Calculator* tool in ArcGIS, version 10 (ESRI 2012). The six most correct surface models, two from each acquisition period (one ascending orbit and one descending orbit) were utilized.

Because only five sample plots were available in this study, the relationship between above-ground biomass and canopy heights was evaluated by dividing the amount of biomass in each plot with the canopy heights in the corresponding plot. The same procedure was used for all six DSMs.

2.4.2 Detection of partially logged areas

This study utilized the DSMs generated from three different time periods, e.g. November 2011, May/June 2012 and November 2012 (Table 3). Hence, DSM height changes could be calculated by subtracting the DSM generated from images acquired in time period 1 from the DSM generated from images acquired in time period 2 ($DSM_{change} = DSM_2 - DSM_1$) using the *Raster Calculator* tool in ArcGIS, version 10 (ESRI 2012).

DSMs matched with ATPM, with images from equal satellite orbits (e.g. image pairs with equal incidence angles) were used in the calculation, in order to exclude the possibility of relative inaccuracies caused by orbit parameters. In addition, the DSMs were corrected for bias according to the results in Table 11.

In addition, reported stand-wise logging volumes from 2011 were used as "ground truth" for visual interpretation of the detected changes. The logging report comprised 22 stands (Table 5.), located near the center of the study area, from which 12 stands had been logged within the time frame of the image acquisitions.

Based on the reported logging in period, I had to estimate the proportion of the logging within the time interval of the Radarsat-2 acquisitions (first acquisition in November, Table 2.). I assumed logging rates were constant, and simply divided the amount of time within the time frame of SAR acquisitions with the total time of the logging period per stand. This factor was then multiplied with the reported logging volume for the corresponding stand (Equation 3.).

Equation 3:

$$VolA = VolR * \frac{TimeA}{TimeR}$$

VolA = volume logged within SAR acquisition period
VolR = reported logging volume
TimeA = logging time within SAR acquisition period
TimeR = reported logging period

Table 5. Overview of the forest stands subjected to logging in 2011. Area in hectares, number of trees, volume in cubic meters. «% in interval» refers to the amount of logging conducted within the time frame of Radarsat-2 acquisitions.

Stand	System	Area	Trees	Volume	Logging period	% in interval
13.AAA	Strip	49.8	802	2991	April - May	0
13.BBB	Strip	105.2	648	2421	October - December	50
13.CCC	Strip	74.9	547	1771	October - December	50
13.DDD	Strip	45.9	543	2442	December	100
13.EEE	Strip	99.1	734	3371	December	100
13.FFF	Selective	58.7	648	2871	September - November	15
13.GGG	Selective	76.3	516	2869	October - November	25
13.HHH	Selective	56.9	491	2394	October - November	25
13.III	Selective	48.5	113	567	July - November	15
13.JJJ	Selective	81	462	2011	October - November	25
13.OO	Strip	102.9	1266	4796	April - December	22
13.PP	Strip	81.1	1694	6139	May - September	0
13.QQ	Strip	113.6	1528	6449	May - September	0
13.RR	Strip	47.4	1172	3784	February - March	0
13.SS	Strip	118.6	1813	6206	April - October	0
13.TT	Strip	76.9	1343	4784	May - September	0
13.UU	Strip	124.4	1435	5629	July - December	21
13.VV	Strip	129.9	1916	6665	July - November	10
13.WW	Strip	135.9	1806	6891	February - July	0
13.XX	Strip	82.2	1046	3400	March - May	0
13.YY	Strip	55.8	748	2417	February - March	0
13.ZZ	Strip	62.6	1040	3848	April - May	0

Visual interpretation of height changes

Visual interpretation of the detected changes in DSM heights was done using a map displaying mean logging volume, i.e. m^3/ha per stand, with graduated colors indicating the logging volumes as estimated with Equation 3.

Based on comparisons with the ground truth map (Figure 21.), the detected changes in DSM heights were assessed as “indeterminable” or “plausible”, studying the pixel values within the delineated stands. Hence, I focused on areas with consistency in terms of red color, i.e. detected negative height change in the DSMs, in order to study if there were correspondence with the ground truth map. Minimum and maximum values were set to -50 and 50 meters, represented by red and green color respectively, in the assessed DSMs (DSM_{CHANGE}) (Figure 22.).

Estimation of logging volumes

Detected changes in DSM heights were used to estimate logged timber volumes by performing simple linear regression analysis, using the DSM_{CHANGE} heights as predictor. The detected changes in DSM heights in the 12 stands that were logged within the time interval of the Radarsat-2 acquisitions were plotted against the calculated logging volumes in the corresponding stands. Detected changes in the DSMs generated from descending orbit image pairs in 6-month and 12-month interval were utilized, i.e. from November 2011 (D0103) to May/June 2012 (D0711) and from November 2011 (D0103) to November 2012 (D1618).

The hypothesis in this analysis was that there would be observed a linear correlation between detected changes in DSM heights and calculated logging volumes. The results provided scatter plots for both time intervals, with trend lines based on the resulting model, using R (R-project 2012). Also, analysis of variance was conducted, using SAS (SAS 2012).

3. Results

3.1 Radargrammetric processing of SAR images

3.1.1 Image matching

The image matching process was evaluated qualitatively by comparing the number of tie points identified and the location accuracy of the tie points (RMSE), i.e. how accurate the tie points in one image are designated to the correct corresponding points in the other image. The number of tie points identified by the operator (IPM) was determined by the user itself, as time was the only limiting factor for how many tie points that could be identified.

Semi-automatic image matching

I was able to identify tie points in all image pairs except from image pair D0105 from November 2011 and image pair D0911 from May/June 2012. The location accuracies of the points, given as RMSE varied from 0.55 pixels to 2.28 pixels, as shown in Table 6. and Table 7. "n/a" means that no tie point could be identified or the location accuracy could not be calculated.

Table 6. Number of Tie Points and location accuracy from semi-automatic image matching on pairs of images acquired in november 2011.

Image pair	Orbit direction	Intersection (degrees)	Tie Points (number)	RMSE (pixels)	Comments
A0204	Asc	13.9	16	0.9	Poor DSM
A0206	Asc	6.2	18	1	Good DSM
A0406	Asc	20.1	10	0.55	Poor DSM
D0103	Desc	11.7	12	0.62	Good DSM
D0105	Desc	26.2	n/a	n/a	No DSM
D0305	Desc	14.5	18	1.23	Poor DSM

Table 7. Number of Tie Points and location accuracy from semi-automatic image matching on pairs of images acquired in May/June 2012

Image pair	Orbit direction	Intersection (degrees)	Tie Points (number)	RMSE (pixels)	Comments
A0810	Asc	20.1	14	0.88	Poor DSM
A0812	Asc	13.9	15	2.28	Poor DSM
A1012	Asc	6.2	15	0.87	Good DSM
A0709	Desc	14.5	18	0.96	Poor DSM
A0711	Desc	11.7	18	0.85	Good DSM
A0911	Desc	26.2	n/a	n/a	No DSM

Automatic image matching

The number of tie points measured by the Adaptive Tie Point Matcher in Socet GXP was in the order of 1 to 27 per image pair. Location accuracies (RMSE) varied from 0.1 pixels to 10.35 pixels (Table 8. to Table 10). However, the location inaccuracy of image pair A0204, i.e. 10.35 pixels was reduced to the same order as the other images, when the matching was run over again. Note the comparability in the results from all three acquisition periods; number of tie points was fairly stable in the «similar» image pairs with respect to number and location accuracy of the tie points.

Table 8. Number of Tie Points and location accuracy from automatic image matching on pairs of images acquired in november 2011

Image pair	Orbit direction	Intersection (degrees)	Tie Points (number)	RMSE (pixels)	Comments
A0204	Asc	13.9	8	10.35	Poor DSM
A0206	Asc	6.2	23	0.17	Good DSM
A0406	Asc	20.1	1	n/a	No DSM
D0103	Desc	11.7	17	0.25	Good DSM
D0105	Desc	26.2	2	n/a	No DSM
D0305	Desc	14.5	6	0.26	Poor DSM

Table 9. Number of Tie Points and location accuracy from automatic image matching on pairs of images acquired in May/June 2012

Image pair	Orbit direction	Intersection (degrees)	Tie Points (number)	RMSE (pixels)	Comments
A0810	Asc	20.1	1	n/a	No DSM
A0812	Asc	13.9	5	0.1	Poor DSM
A1012	Asc	6.2	20	0.27	Good DSM
D0709	Desc	14.5	1	n/a	No DSM
D0711	Desc	11.7	18	0.28	Good DSM
D0911	Desc	26.2	1	n/a	No DSM

Table 10. Number of Tie Points and location accuracy from automatic image matching on pairs of images acquired in november 2012

Image pair	Orbit direction	Intersection (degrees)	Tie Points (number)	RMSE (pixels)	Comments
A1315	Asc	20.1	n/a	n/a	No DSM
A1317	Asc	13.9	5	0.07	Poor DSM
A1517	Asc	6.2	27	0.3	Good DSM
D1416	Desc	26.2	1	n/a	No DSM
D1418	Desc	14.5	2	n/a	No DSM
D1618	Desc	11.7	18	0.29	Good DSM

3.1.2 Generation of Digital Surface Models

Visual interpretation

All surface models were assessed as «reasonable» due to the fact that they represent at least an approximation of what we could consider to be the actual surface, here compared with the SRTM 30 meter grid «reference DSM». However, only the best DSMs from each orbit were considered good enough for further quality analysis. These were A0206 and D0103 from November 2011, A1012 and D0711 from May/June 2012, and A1517 and D1618 from November 2012.

These six digital surface models provided more details of the surface, in contrast to the rest of the DSMs which were more indistinct. In addition to blurred surface properties, some artifacts, i.e. break lines were observed in the «poor» DSMs, especially near the left and right edges of the scene. Similar image combinations from all three acquisition periods resulted in similar digital surface models, with respect to visual attributes. Hence, Figure 19. and Figure 20. comprise only the DSMs from the first acquisition period, i.e. November 2011, but they are representative for the DSMs generated from image pairs acquired in May/June 2012 and November 2012 as well.

The image pair with the lowest intersection angles from both ascending (e.g. 6.2 degrees in A0206) and descending orbits (e.g. 11.7 degrees in D0103) generated the most correct digital surface model, whereas D0103 appeared to give the best representation of the surface. The image pairs with the largest intersection angle among the image pairs (e.g. 26.2 degrees, from descending orbits) did not result in any DSM at all. The rest of the models were assessed to be of poor quality, based on the visual representation (Figure 19 and 20). Also, note the comments for all image pairs in Table 6. to Table 10.

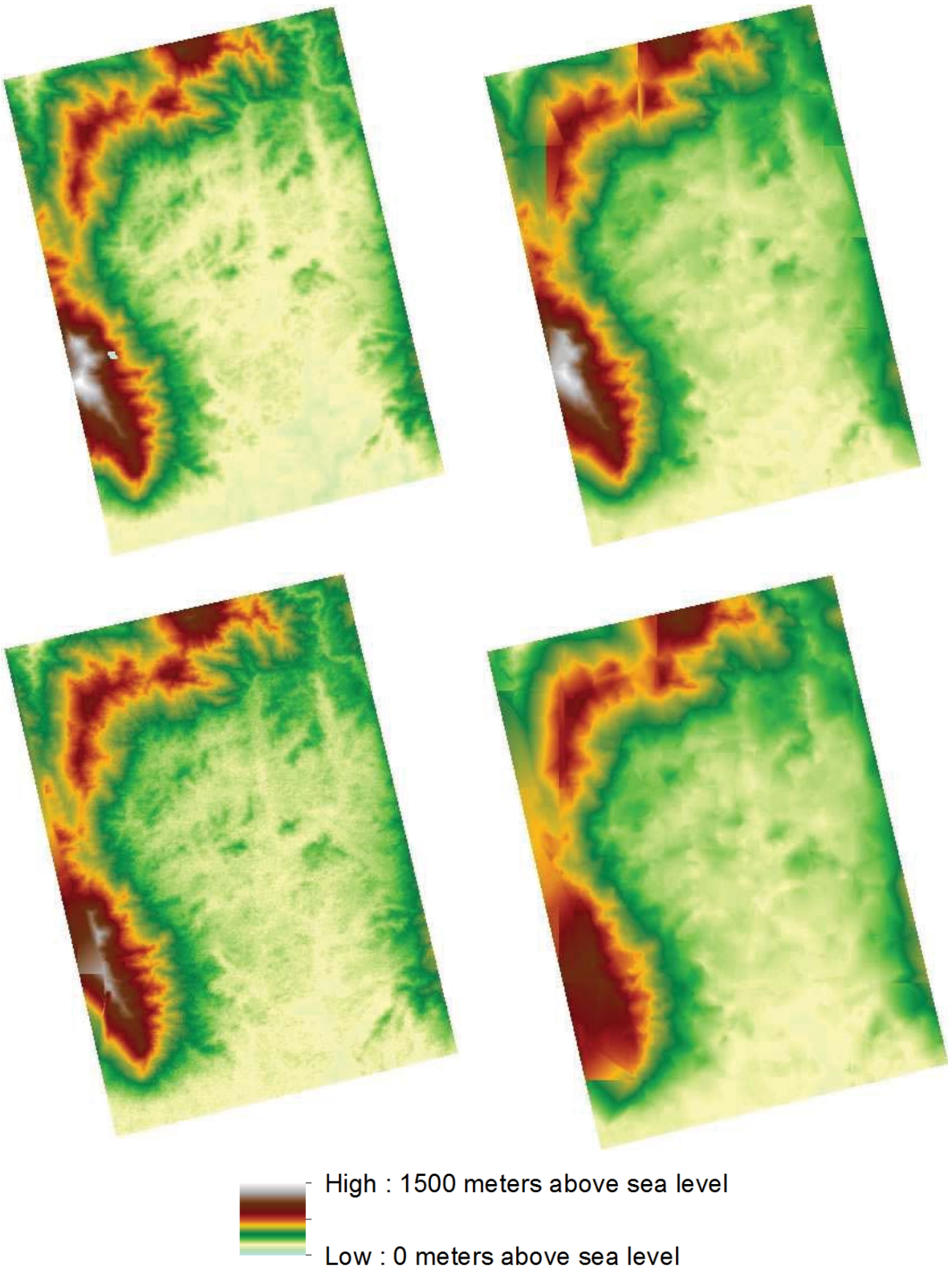

Figure 19. Digital Surface Models (DSMs) from ascending orbit acquisitions. SRTM "reference DSM" (upper left), DSM A0204 (upper right), DSM A0206 (lower left) and DSM A0406 (lower right). These samples demonstrate the DSMs from all acquisition periods, as the same orbits were used repeatedly, thus providing similar visual properties.

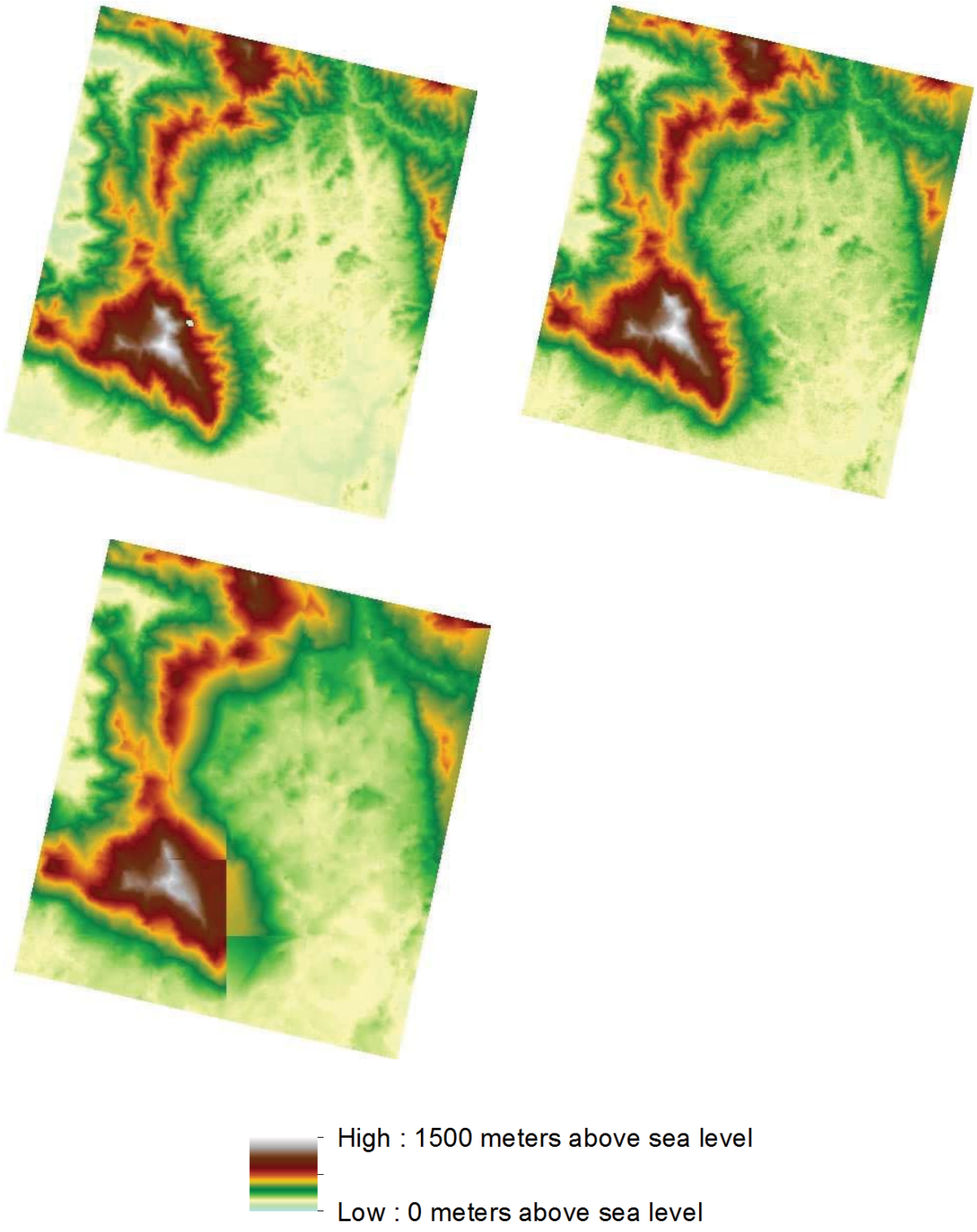

Figure 20. Digital Surface Models (DSMs) from descending orbit acquisitions. SRTM "reference DSM" (upper left), DSM D0103 (upper right), DSM D0709 (lower left). Image pairs with These samples demonstrate the DSMs from all acquisition periods, as the same orbits were used repeatedly, thus providing similar visual properties.

Assessment of height accuracy

Regarding image pairs matched with IPM (A0206 and D0103), mean height deviations (bias) were calculated to 0.2 and -9.3 meters, root mean square error (RMSE) 5.5 and 15.5 meters and standard deviation 5.9 and 13.3 meters respectively, compared to the independent check points (ICPs), calculated by Socet GXP (Table 11.).

Image pairs matched with ATPM had bias ranging from -0.2 (A0206) to 34.6 meters (D0711), RMSE from 5.5 to 35.4 meters and standard deviation from 3.7 to 12.8 meters.

The utilization of a ground control point (GCP) in image pair A0206 and D0103 did not improve the height accuracy, and actually in some cases the GCP only contributed to a worse result (Table 11.).

Table 11. Height accuracy check of the most correct DSMs, compared with 8 independent check points (ICP). Height deviations dZ = Z_{ICP} - Z_{DSM}, hence a negative dZ means the DSM heights are higher than the ICP heights. Values in meters. Bias = mean height deviation. Strat refers to the image matching strategy, where I = IPM, A = ATPM, G = GCP

Image pair	Strat	ICP 1	ICP 2	ICP 3	ICP 4	ICP 5	ICP 6	ICP 7	ICP 8	Bias	RMSE	StD
A0206	I	-9.2	10.2	-4.8	2.9	4.1	-1.8	0.7	0.7	0.3	5.5	5.9
	A	-10.1	9.7	-3.6	3.4	0.2	-3.2	2.8	-0.3	-0.2	5.5	5.8
	A + G	-10.3	9.8	-4.8	2.5	9.4	-3.6	3.7	-1.6	0.7	6.6	7.0
D0103	I	-14.1	0.6	-4.0	-5.3	-39.5	-10.1	-4.2	2.1	-9.3	15.5	13.3
	A	-13.8	4.1	-4.0	-6.5	-37.0	-9.6	-5.0	2.2	-8.7	14.8	12.8
	A + G	-14.2	4.2	-3.9	-5.6	-23.1	-9.7	-3.1	2.3	-6.7	10.7	8.9
A1012	I	-27.9	-3.6	-24.9	-8.8	-24.1	-18.9	-6.0	-16.4	-16.3	18.5	9.3
	A	-23.3	-7.2	-20.2	-6.9	-24.0	-21.3	-16.6	-16.4	-17.0	18.1	6.7
D0711	I	-39.5	-22.8	-33.3	-36.9	-40.0	-28.2	-28.7	-33.3	-32.8	33.3	6.0
	A	-39.4	-22.1	-34.6	-36.7	-50.3	-28.8	-29.0	-35.5	-34.6	35.4	8.4
A1517	A	-29.3	-3.7	-25.7	-6.2	-21.3	-16.5	-8.5	-18.5	-13.8	15.3	7.1
D1618	A	-12.8	-4.5	-16.8	-13.8	-12.4	-15.3	-11.0	-13.0	-12.5	12.9	3.7

3.2 Applications in tropical forest monitoring

The application of the DSMs for tropical forest monitoring was evaluated with two different approaches. Firstly, the relationship between above-ground biomass and canopy heights was evaluated, by dividing the amount of biomass in each plot with the corresponding canopy height model (CHM) extracted from all image pairs. This evaluation resulted in fairly plausible values.

Secondly, DSMs generated from multiple image pairs acquired with 6 months interval over a time frame of one year (three acquisition periods) were utilized, with the purpose of correlating detected changes in DSM heights and the calculated logging volumes.

3.2.1 Relationship between above-ground biomass and canopy heights

Table 12 presents the amount of biomass per meter canopy height estimated in the five sample plots with the utilization of the six DSMs.

The relationship between above-ground biomass and height of the canopy height models varied between approximately 4 t/ha/m and 45 t/ha/m.

Average value for the canopy height models combined was 13.5 t/ha/m, with one significant outlier from CHM A0206 / Plot 7r removed (Table 12.).

Table 12. Amount of above-ground biomass estimated per meter CHM height in each sample plot (left-hand coloumn), estimated with the various digital surface models (top row). Values in tons/hectare per meter

Plot	A0206	D0103	A1012	D0711	A1517	D1618	Averaged
6cc	19.4	11.6	7.6	5.2	9.8	11.0	10.7
6dd	12.6	7.1	6.3	4.3	6.2	8.9	7.3
7q	7.1	23.8	11.0	6.7	8.4	19.9	11.4
7r	1161.6	25.4	13.5	3.9	8.8	23.0	242.7
7v	33.2	46.2	11.4	9.0	11.8	14.7	22.3
Average	246.8	22.8	10.0	5.8	9.0	15.5	

3.2.2 Detection of partially logged areas

Visual interpretation

The ascending orbit DSMs (Figure 22, top) was influenced by much noise, while the descending orbit DSMs (Figure 22, bottom) showed in general a tendency of comparability with the ground truth map. Thus, the former were assessed «indeterminable» and the latter were assessed «plausible», compared to the ground truth map (Figure 21.).

However, some of the stands that supposedly were not logged had a detected reduction in DSM height. Some of this may be due to noise or inaccuracies in the utilized DSMs, and it appeared as the DSMs from ascending orbits were affected by more noise than the DSMs from descending orbits. In either case, actual logging outside the reported time frame or even illegal logging could not be excluded as a possible explanation of the observations.

Reduced heights were observed in both strip-logged stands as well as selective-logged stands, indicating the ability to detect partially logging. The 1-year changes from November 2011 to November 2012 were fairly similar to the 6-month changes from November 2011 to May/June 2012, indicating a general termination of logging activity, as in compliance with the logging reports.

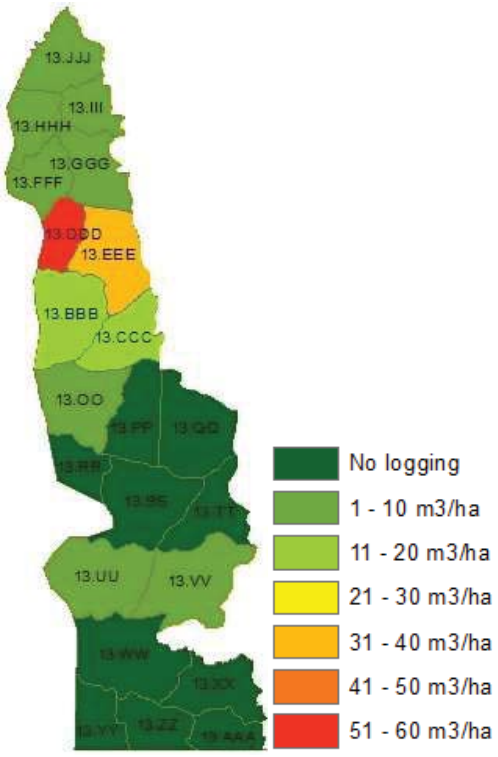

Figure 21. "Ground truth" map showing the reported logging activity from November 2011 to November 2012. Logging volumes showed in graduated colors.

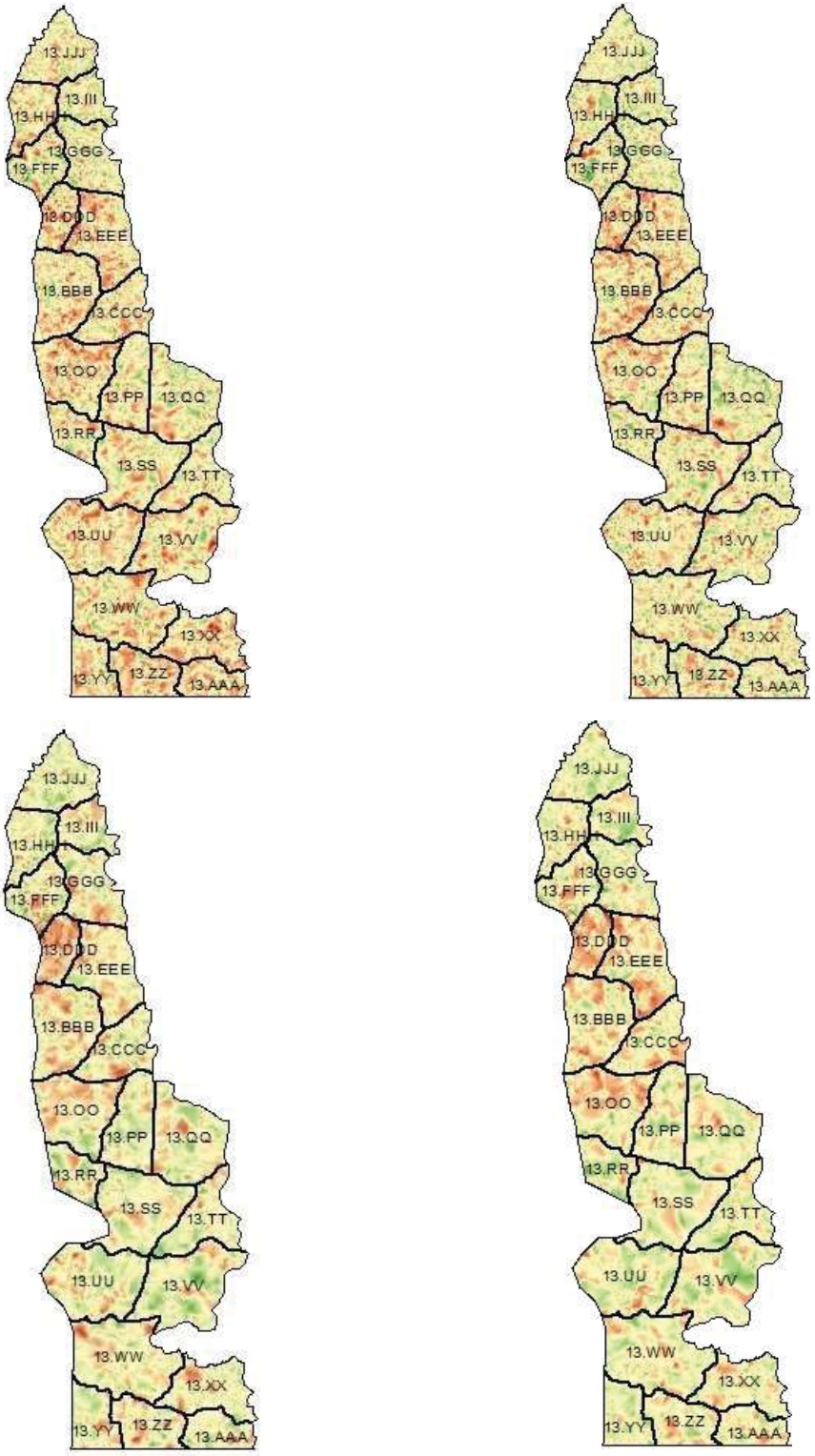

Figure 22. Visual representation of observed changes in DSM heights from November 2011 to May/June 2012 (left side maps) and November 2011 to November 2012 (right side maps). Ascending orbits on top, descending orbits bottom.

Estimation of logging volumes

The resulting model from the 6-month correlation provided a slope of -2.5 (Figure 23.). This means, 1 meter detected reduction in DSM height corresponded to a mean logging volume of 2.5 m^3/ha per stand. The standard error was 0.5 m^3/ha.

The intercept was 9.8 m^3/ha with a standard error of 2.5 m^3/ha.

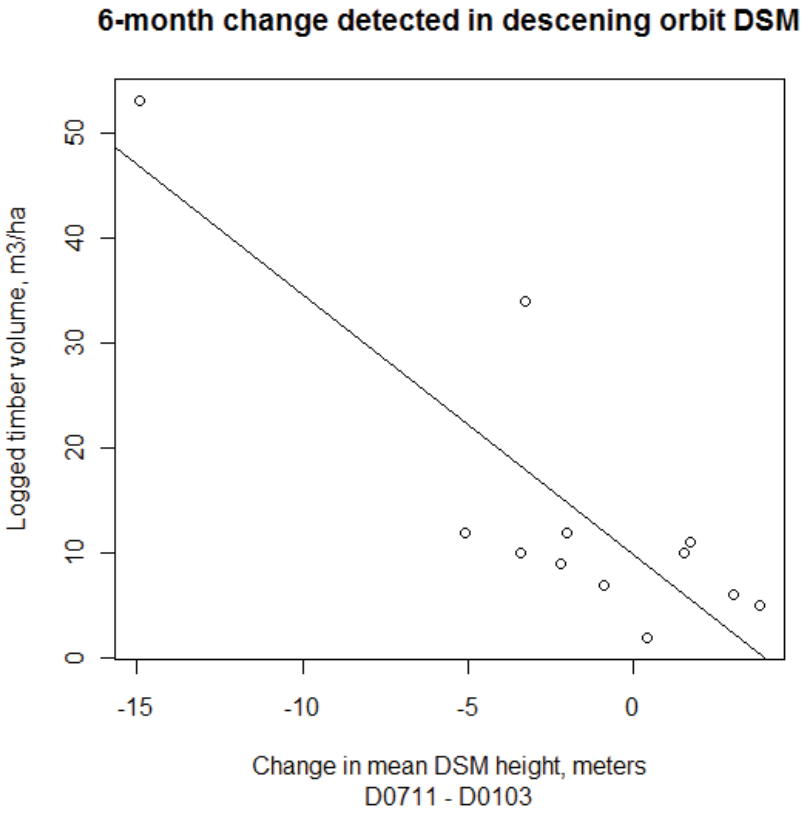

Figure 23. Correlation between stand-wise logging volume and detected changes in DSM heights from November 2011 to May/June 2012. DSMs generated from descending orbit image pairs.

Analysis of variables (Table 13.) showed that the correlation factor (R^2) was 0.71 (i.e. sum of squares from model divided with total sum of squares) and RMSE was approximately 8.2 m^3/ha or 57.5 % (RMSE %). F-value was 25.03 with a level of significance of 0.0005.

Table 13. Analysis of variance of the model predicting stand-wise logging volumes with detected changes in DSM heights from November 2011 to May/June 2012.

Source	DF	Sum of squares	Mean square	F-value	Pr > F
Model	1	1676.686155	1676.686155	25.03	0.0005
Error	10	669.912735	66.9912735		
Corrected total	11	2346.59889			

The resulting model from the 12-month correlation also provided a slope of -2.5 (Figure 24.). This means, 1 meter detected reduction in DSM height corresponded to a mean logging volume of 2.5 m^3/ha per stand. The standard error was 0.5 m^3/ha.

The intercept was 10.4 m^3/ha with a standard error of 2.5 m^3/ha.

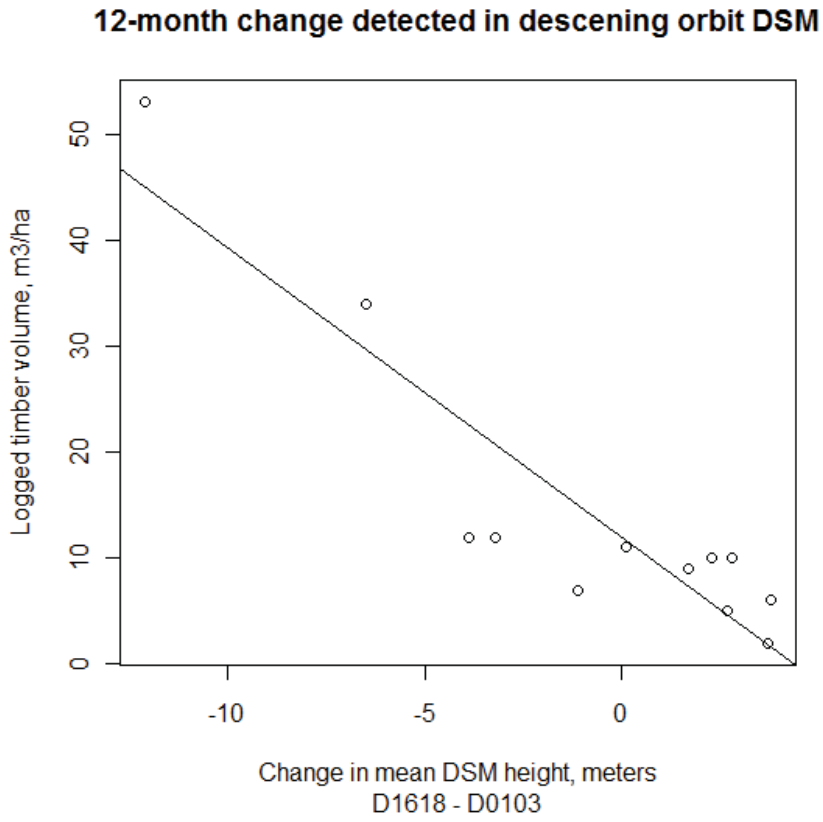

Figure 24. Correlation between stand-wise logging volume and detected changes in DSM heights from November 2011 to November 2012. DSMs generated from descending orbit image pairs.

Analysis of variables (Table 14.) showed that the correlation factor (R^2) was 0.72 (i.e. sum of squares from model divided with total sum of squares) and RMSE was approximately 8.1 m^3/ha or 56.6 % (RMSE %). F-value was 26.15 with a level of significance of 0.0005. The correspondence of the two models indicated a termination of logging activity after the first 6 months.

Table 14. Analysis of variance of the model predicting stand-wise logging volumes with detected changes in DSM heights from November 2011 to May/June 2012.

Source	DF	Sum of squares	Mean square	F-value	Pr > F
Model	1	1697.520235	1697.520235	26.15	0.0005
Error	10	649.078656	64.9078656		
Corrected total	11	2346.598891			

4. Discussion

The outline of this study featured three main objectives, which in overall would investigate the methods of radargrammetric processing of SAR images, and the application of radargrammetric surface models in tropical forest monitoring. Although the objectives were separated, the findings in the study of the methods were influenced by relevant findings in the study of the application, and vice versa. Hence, there were probably connections between the results from the different objectives. However, I am aware of the possibility of a «confirmation bias», i.e. that the search for strong correlations may influence the interpretation of the results.

The data sets were in general influenced by uncertainty, and two main problems were evident through the study; the quality of the field data and the uncertain absolute location accuracy in Radarsat-2 SAR imagery.

4.1 Radargrammetric processing of SAR images

In this study I used a commercial software package; namely Socet GXP from BAE Systems. Software packages from competing suppliers were considered prior to the study, but based on the desire to experiment with untested software, combined with the fairly easy to use graphical user interface of Socet GXP, the latter was chosen. Several settings were tested in Socet GXP, in order to be confident that potential errors in the radargrammetric processing were not caused by the software or the incorrect use of any module. As this study did not address the software itself, and extensive documentation was lacking, potential software related issues could not be sorted out. However, it would be interesting to test competing software packages as well, and study if the use of alternative solutions would have provided different results from what I got.

4.1.1 Image matching

The processing results varied considerably between the image pairs. The image pairs with higher incidence angles, i.e. closer to horizontal, combined with small intersection angle generated the most correct surface models, and were also the image pairs with the highest numbers of tie points identified by ATPM. However, there were no obvious connections between matching result (number and location accuracies of tie points) and the quality of the DSMs that were generated, because the «poor» DSMs had no improved visual quality although I was able to identify more tie points in these image pairs using IPM. This may

indicate that the acquisition properties themselves, i.e. incidence- and intersection angles are more important factors than the results from the image matching.

Semi-automatic image matching

It should be noted that the number of tie points identified visually was no independent result, as the result would have been affected by the time spent in searching for corresponding points. However, the experiences from visual identification of tie points were valuable as the differences due to varying image properties could be studied.

It was easier to detect infrastructure in scenes acquired from higher incidence angles and thus easier to identify tie points visually. This observation was supported by the different properties of SAR images acquired from different incidence angles, as discussed in chapter 2.3.1. Also, it was easier to identify tie points in corresponding images when the intersection angles were small. Toutin & Gray (2000) made a similar conclusion.

The location accuracy of the tie points was fairly stable in all image pairs. Hence, I believe that as long as tie points could be identified, the location accuracy was fairly good, i.e. in the order of sub-pixel. Outliers may have occured, and hence some local variations in terms of DSM quality may be expected. The latter was not further analyzed, however.

Automatic image matching

DSMs could not be generated from image pairs with intersection angles greater than 14.5 degrees, as ATPM was unable to identify sufficient number of tie points (Table 8. to Table 10). This is interesting, as it was possible to generate DSMs from the equivalent image pairs when I used IPM.

I believe one of the main advantages of sophisticated image matching software packages is the ability to perform the matching automatically. However, the human brain proves able to see patterns on a higher level. Location accuracies may be slightly worse in image pairs matched with IPM. Nevertheless, I believe it was possible to generate DSMs because I was able to identify more tie points in the image pairs with higher intersection angles, than ATPM was able to.

4.1.2 Generation of Digital Surface Models

The DSMs were generated using the NGATE module of Socet GXP. Karjalainen et al. (2012) also used NGATE, and although they used the same module in GXP's predecessor, i.e. Socet SET (version 5.5) I believe the performance of the NGATE module has remained equal.

All DSMs were generated with the following output properties: 10x10 meter pixel size, WGS84 as horizontal reference system, and geoid heights, i.e. heights referred to as meters above sea level. The height values in some of the datasets were referenced to the WGS84 ellipsoid. Hence, I had to be cautious when subtracting DSMs from another, and be sure the ICPs were in the correct reference system. In fact, this was an important lesson learned, as I spent much time verifying heights in the beginning. The mean geoid height, i.e. height above sea level in the study area was approximately 42 meters above the WGS84 ellipsoid (NGA 2012).

Visual interpretation

Visual interpretation of DSMs was also performed by (Demir 2010). The study showed that the differences between the generated DSMs were large in high relief areas, i.e. mountainous topography, when compared to a global DEM (GDEM). Hence, the location of my study area had an important role in interpretation of such topography, as most of the high relief areas in SBK were located in the outskirts of the SAR images, thus making a qualitative interpretation in this manner unfeasible. Study of high relief areas would hence be an interesting subject in a future study. I observed that the DSMs were more inconsistent in the left and right edges. This may have been caused by lack of overlapping areas due to the difference in incidence angles, which in turn lead to inability to generate precise height values in these areas.

The visual interpretation performed in this study revealed that DSMs generated from image pairs with smallest intersection angles, i.e. 6.2 and 11.7 degrees in the image pairs from ascending and descending orbits, respectively were most correct. As discussed by (Toutin & Gray 2000), intersection angles should be small, in order to obtain good image matching. Paradoxically, intersection angles should be large in order to obtain good geometry for height computation.

The difficulties in image matching caused by too large intersection angles is a possible reason why the image pairs I utilized that had larger intersection angles, i.e. 13.9 to 26.2 degrees generated DSMs with poor representation of the topography, as well as having artifacts, i.e. visible break-lines. The advantage of large intersection angles, i.e. good geometry for height

computation, is a possible explanation of why descending image pairs with intersection angle 11.7 degrees generated more correct DSMs than ascending image pairs with 6.2 degrees intersection.

Hence, the possibility of a “threshold value” in intersection angles, i.e. somewhere between 11.2 and 13.9 degrees, for generation of the most correct DSMs could not be excluded. However, more image pairs comprising a greater variety of incidence angles would be needed in order to conclude on this theory. Also, the poor visual attributes may not only be induced by a large intersection angle alone. The image pairs with one image acquired with a low incidence angle, i.e. 24.7 and 21.7 degrees for ascending and descending orbits respectively, may have poor visual attributes caused by the problems in matching images with large differences due to the properties of the images with low incidence angle, as demonstrated in Figure 15.

Accuracy assessments

Height accuracy assessments revealed that image pair A0206 matched with ATPM had the smallest errors. Note that image pairs with small intersection angle also were the image pairs generating “good DSMs” (Table 6. to Table 10.).

Assessment of height accuracies were performed utilizing 8 independent check points (ICPs). All ICPs were located in an elevation interval of approximately 160 meters. Hence, high relief areas, i.e. mountainous topography surrounding the study area were not subjected to assessments of height accuracy. This would have been interesting, since elevation values are expected to be more uncertain in high relief areas (Demir 2010; Toutin & Gray 2000).

The check points were measured by means of differential GPS (dGPS), and hence the absolute locations of the ICPs were assessed being accurate. This was simply because I was not able to assess them otherwise, and from some point the field data will have to be trusted as «ground truth». However, the differences in height deviations between the DSMs were noticeable, and questions about what was causing the observed differences may be raised. Plausible but not verified explanations include the effects from weather conditions in the SAR images, and in particular the amount and variations of moisture on backscattering surfaces, e.g. soil, leaves and branches (Wagner et al. 2008). Weather conditions during the SAR acquisitions are reported in Table 2. Although varying conditions occurred, no clear correlation could be seen based on the observations.

The possibility of relative inaccuracies in SAR image acquisitions due to «drift off» in the positioning of the satellite may not be excluded, as Radarsat-2's positions are calculated with the use of onboard GPS devices. Also, the inherent properties of SAR images in SGF-format imply an absolute location error of up to 15 meters (Slade 2011). However, the DSM heights measured in ICP5 (Figure 25) were as high as 50 meters above the ICP (DSM D0711), and thus the absolute location error induced by Radarsat-2 did not solely stand out as an explanation of the height deviations.

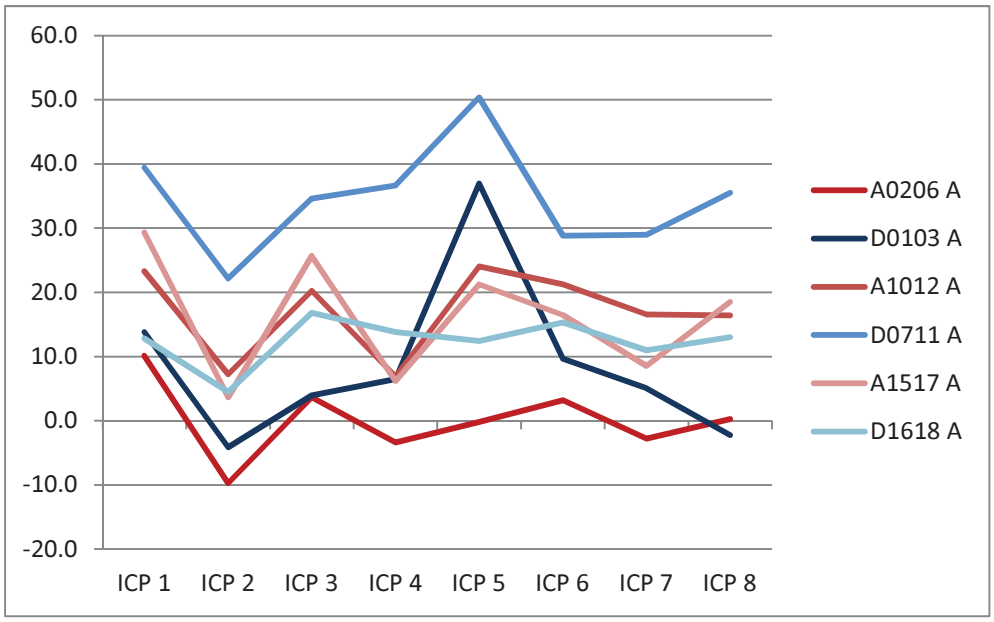

Figure 25. Line chart showing the height deviations (dZ) of DSMs generated from image pairs A0206, D0103, A1012, D0711, A1517 and D1618. All image pairs matched with ATPM without GCP. Values on Y-axis in meters. ICP heights (Z_{ICP}) = 0. Data from Table 11.

Ground Control Points

Proper quantities of ground control points (GCPs) with good quality may significantly improve the location accuracies of DSMs (Toutin & Gray 2000). In my study, one GCP was utilized. The use of one GCP did not improve the location accuracies significantly, however.

If more GCPs, (i.e. points that have XY- and/or Z-coordinates and are definite in the SAR images) were measured, better assessments of the height accuracies could have been performed. This is because the DSMs then could have been corrected for inaccuracies in planimetry, i.e. X (easting) and Y (northing), thus adding certainty to the comparability of the height values.

Also, the planimetric accuracies could have been assessed utilizing GCPs. Hence, the efforts made in measuring GCPs with number and quality can in general not be underestimated, as the utilization of GCPs may not only improve absolute location accuracies when utilized in the radargrammetric processing, but also be utilized for quantitative assessments of accuracies in X, Y and Z after the generation of DSMs.

Accurate DSMs can also be generated without GCPs (Toutin & Omari 2011; Toutin 2012). However, this was not among the objectives in this study, and hence no efforts were made in attempting to improve the location accuracies of the generated DSMs.

Height interpolation bias

Based on the observed height deviations, I would also like to introduce another theory of what may be causing the measured height deviations in the ICPs; namely a bias due to height interpolation, i.e. the «stiffness» of the generated DSMs (Figure 26.). The DSMs were generated with an output pixel size of 10x10 meters. The typical width of the roads in the study area of up to 10 meters, combined with the abrupt elevation differences imposed by the roads, i.e. 20 meter (and higher) forest canopy heights close to the roads, may possibly explain the height deviations, caused by height interpolations in the generated DSMs. The DSMs were generated over again, with less output pixel size, i.e. 3 meters. However, this effort did not affect the height deviations at all, and hence I was not able to point at any software properties as an underlying cause of the height deviations in the DSMs.

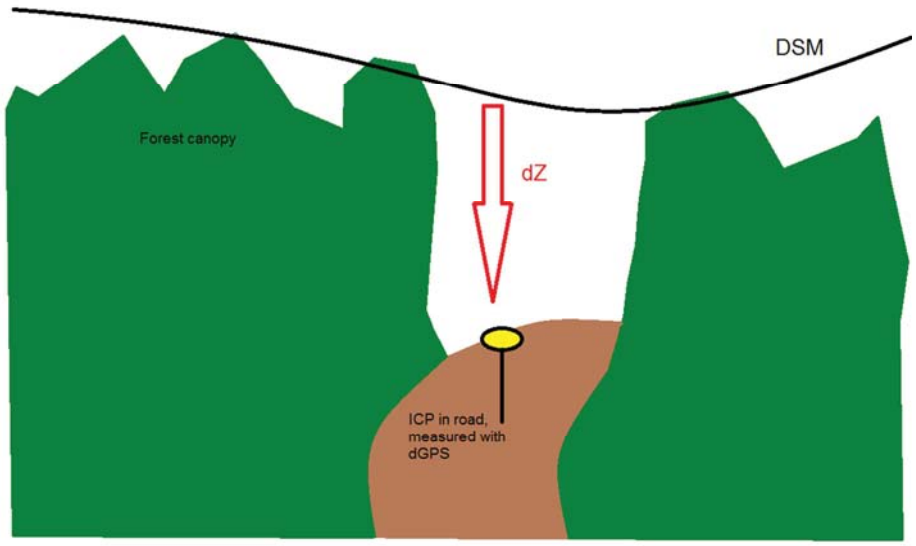

Figure 26. The principle of the height deviations (dZ) caused by the assumed "stiffness" of the generated DSMs. The combination of ICPs located in relative narrow roads, i.e. typically 10 meters wide and the «stiffness» of the generated DSMs is assumed to cause height deviations, as the DSM is not able to "«dip" down in the road.

While height interpolations might explain the general overestimation of DSM heights compared to the ICPs, it should be noted that this is only a vague assumption based on the fact that the DSMs that had large height deviations were predicting more plausible amounts of biomass per meter CHM than the DSMs with less height deviations (Tables 11 and 12), and I was not able to figure this out.

4.2 Applications in tropical forest monitoring

4.2.1 Relationship between above-ground biomass and canopy heights

Results

Amounts of above-ground biomass were divided with CHMs make approximations in the relationship between them, a lot more uncertain approach than a regression analysis of the relationship. However, as the number of observations was too low, this approach was chosen simply to demonstrate the approximate biomass values provided by radargrammetric surface models in tropical forest areas.

The average amount of above-ground biomass per meter CHM in the five sample plots was in the order of 13.5 tonnes/ha (Table 12), fairly close to what was observed by Solberg et al. (2010). It should be noted that the latter study was not applied in tropical forests. However, I will at least consider the observed values in my study as plausible. Also, based on my own experience from the study area, considerably amounts of biomass were probably not taken into account due to the complex structures in tropical forests. I believe approximately 75 % of the total above-ground biomass was calculated, as the field data that were provided, i.e. the inventory data, did only consist of trees above 10 cm DBH. The forest inventory of the sample plots was conducted in 2008; hence the possibility of errors due to forest growth could not be disregarded.

Alternative approach

In order to increase the number of observations, i.e. more than the five sample plots, another approach were attempted in the beginning of the study; namely «gridding» the sample plots into 16 equal square cells, i.e. 25x25 meters (625 m^2) per cell. The location of every single tree in the sample plots made this possible, i.e. both above-ground biomass and canopy heights were calculated for all 16 cells within each sample plot. However, this proved unfeasible, as no obvious correlation could be interpreted from the resulting scatter plots.

Explanations of this include the possibility of a height interpolation bias, i.e. DSM «stiffness», as well as the size of the cells. Although tree locations are accurate, the interaction between biomass and SAR signals may act different due to canopy closure; due to the complex structures in the tropical forests, i.e. branches from trees may «stretch into» neighboring cells, and could cause errors in the approximation of biomass, as the measured canopy height in one cell may correspond to the biomass of a tree located in another cell. Also, although the contour lines provided for the sample plots seemed plausible, the true terrain heights within one sample plot remained uncertain. One solution to this problem could have been accurate DTMs generated from LiDAR acquisitions; however, LiDAR acquisitions were not an option in this particular study.

Tree heights

The tree heights were not measured, and thus height values were estimated with the use of an allometric function. However, (Basuki et al. 2009) demonstrated that the inclusion of measured tree heights did not have any significant improvement on the biomass estimation.

One should still be aware of the uncertainty imposed by the use of allometric biomass estimations, especially as the development of the functions are not properly documented in terms of scientific results. But again, the allometric biomass equations used in this study were developed specifically for the use in SBK, and hence I regarded them applicable, given they were correctly applied. Also, the estimation of absolute biomass values was of relatively low importance, as the general uncertainty in the datasets supposedly would provide results that could not be concluded too surely upon.

4.2.2 Detection of partially logged areas

Detection of partially logged areas and estimation of logging volumes by studying temporal changes in DSM heights from radargrammetric surface models were previously not demonstrated by anyone, as far as I know. Hence, there are no equivalent studies to compare my results with. Although uncertainties affected my work, the results were promising.

Visual interpretation

The two DSM_{CHANGE} generated from ascending orbit image pairs were in general noisier than the two generated from descending orbit image pairs. A possible explanation is the low intersection angles in the ascending orbit image pairs, i.e. 6.2 degrees. In contradiction, the descending orbit image pairs had higher intersection angles, i.e. 11.2 degrees. Higher

intersection angles are recommended in order to make good parallax calculations and thus height calculations (Toutin & Gray 2000).

Regardless of any observed noise, the various DSM_{CHANGE} (Figure 22.) compared to the ground truth map (Figure 21.) indicated a correlation between the detected changes in DSM heights and the logging volumes. Although eventual random errors remained uncertain, and they could influence the result, this was a promising result that indicated a possibility of detecting partially logged areas by means of repeated use of radargrammetric surface models.

Estimation of logging volumes

The simple linear regression models provided fairly good correlations between detected changes in DSM heights and stand-wise logging volumes. The utilized DSMs were corrected for mean height deviations according to Table 11. The model representing the 12-month time interval had a slightly better correlation than the model representing the 6-month time interval. This means there could have been some differences between the models that might indicate logging activity after the first six months. However, the difference was not significant. Also, a general termination of logging activity after the six first months was anticipated, in compliance with the logging reports.

Only the 12 stands that were reportedly logged within the time interval of the Radarsat-2 image acquisitions were utilized in the correlation, as no logging in some stands would cause the slope of the correlation to flatten. However, changes in DSM heights were detected in the stands that were not included, and hence it was hard to determine which would be the most correct correlation.

The estimated logging volumes per meter DSM_{CHANGE} (Chapter 3.2.2) were fairly low compared to the observed amounts of biomass in Table 12, given a wood density of 0.6 – 0.7 $tons/m^3$ (Basuki et al. 2009). This is in conflict with the introduced theory of height interpolation bias, as the logging volumes should have been overestimated due to relatively low detected changes in DSM heights. However, the CHMs providing fairly high amounts of above-ground biomass in Table 6. were not corrected for bias, and hence the estimated amounts of above-ground biomass could well be overestimated. Also, the effects imposed by eventual random errors must be taken into consideration, as the possibility of errors caused by the complex structures in tropical forests could not be excluded.

4.3 Recommendations for future studies

Future research could include the generation of radargrammetric DSMs in high relief areas. The DSMs I generated covered a relatively flat area only surrounded by higher ridges, and hence I cannot conclude whether the methods were applicable to areas of mountainous areas, a type of topography that is often seen in Central Kalimantan.

The lack of GCPs with number and quality and the generally uncertain location accuracies in this study led to an assumption that more GCPs could have provided sufficient certainty in relative as well as absolute location accuracies of DSMs generated from Radarsat-2 image pairs, as demonstrated in several studies (Toutin & Gray 2000; Toutin 2010). Sufficient location accuracy without the use of GCPs is also feasible (Toutin & Omari 2011). However, the latter approach would require more extensive experience with radargrammetric processing of SAR images. Utilization of other sensors could be an alternative for providing sufficient location accuracy without using GCPs may be possible, as preliminary results from radargrammetric processing of TerraSAR-X image pairs in the NGATE module, even without identification tie points, are promising (Weydahl 2012).

Proper planning of future studies should be focused on, with emphasis on selecting study areas with sufficient field data in terms of forest inventories and the availability of good DTMs. Also, longer time-series of both SAR acquisitions and field inventories could provide better understanding of temporal changes in DSM heights, given that the SAR acquisitions may be influenced by weather conditions as well as “drift-off” in location accuracy.

5. Conclusions

This study demonstrated the application of radargrammetric surface models from Radarsat-2 Ultrafine SAR images with 3 meter resolution for forest monitoring.

Two main problems affected this study; the quality of the field data, i.e. the number and location accuracies of sample plots, and inaccuracy in Radarsat-2's orbital data. Hence, the potential of radargrammetry could not be demonstrated to the full.

However, with the use of repeated DSMs generated from image pairs acquired from the same satellite orbits, detection of partially logged stands was achievable, supporting the applicability of radargrammetric surface models in forest monitoring.

My conclusions are:

a) Image pairs from descending orbits with mean incidence angles of 47.9 and 36.2 degrees, thus with intersection angle 11.7 generated the best DSMs

b) A detected increase of 1 meter canopy height corresponded to between 4 and 45 t/ha increase in above-ground biomass

c) Partial logging, both strip-logging and selective logging can be detected as change in repeated radargrammetric DSMs, and the relationship between reported logging quantities and the decrease in DSM heights in the corresponding time interval was plausible

References

Anonymous. (2008). *Synthetic Aperture Radar Land Applications Tutorial, Part I: Background and Theory*: European Space Agency, Sarmap, UNESCO. Available at: http://earth.eo.esa.int/download/eoedu/Earthnet-website-material/to-access-from-Earthnet/2008_Bilko-SAR-Land-Applications-Tutorial/sar_land_apps_1_theory.pdf (accessed: November 29th, 2012).

BAE. (2012). Available at: http://www.geospatialexploitationproducts.com/content/products/socet-gxp (accessed: November 11th, 2012).

Balzter, H. (2001). Forest mapping and monitoring with interferometric synthetic aperture radar (InSAR). *Progress in Physical Geography*, 25 (2): 159-177.

Basuki, T. M., van Laake, P. E., Skidmore, A. K. & Hussin, Y. A. (2009). Allometric equations for estimating the above-ground biomass in tropical lowland Dipterocarp forests. *Forest Ecology and Management*, 257 (8): 1684-1694.

Canadell, J. G. & Raupach, M. R. (2008). Managing forests for climate change mitigation. *Science*, 320 (5882): 1456-1457.

De Oliveira, C. G., Paradella, W. R. & da Silva, A. D. (2011). Assessment of radargrammetric DSMs from TerraSAR-X Stripmap images in a mountainous relief area of the Amazon region. *ISPRS Journal of Photogrammetry and Remote Sensing*, 66 (1): 67-72.

Demir, M. A. S., E.; Musaoglu, N.; Örmeci, C. . (2010). *Accuracy assessment of radargrammetric DEM derived from Radarsat-2 ultrafine mode* ISPRS Istanbul Workshop 2010 on Modeling of optical airborne and spaceborne Sensors.

ESRI. (2012). *ArcGIS*. Available at: http://www.esri.com/software/arcgis (accessed: November 13th, 2012).

Fayard, F., Meric, S. & Pottier, E. (2007, 23-28 July 2007). *Matching stereoscopic SAR images for radargrammetric applications*. Geoscience and Remote Sensing Symposium, 2007. IGARSS 2007. IEEE International. 4364-4367 pp.

Freeman, T. (1996). *What is imaging radar?* Available at: http://southport.jpl.nasa.gov/desc/imagingradarv3.html (accessed: November 7th, 2012).

Fuller, D. O. (2006). Tropical forest monitoring and remote sensing: A new era of transparency in forest governance? *Singapore Journal of Tropical Geography*, 27 (1): 15-29.

Gama, F. F., Dos Santos, J. R. & Mura, J. C. (2010). Eucalyptus Biomass and Volume Estimation Using Interferometric and Polarimetric SAR Data. *Remote Sensing*, 2 (4): 939-956.

Gibbs, H. K., Brown, S., Niles, J. O. & Foley, J. A. (2007). Monitoring and estimating tropical forest carbon stocks: making REDD a reality. *Environmental Research Letters*, 2 (4).

Holmgren, P. C., T.; Kasten, T. (2008). Role of satellite remote sensing in REDD: UN-REDD Programme, Food and Agriculture Organization of the United Nations, United Nations Development Programme, United Nations Environment Programme.

Ismail. (2012). *Personal communication* (December 6th, 2012).

Karjalainen, M., Kankare, V., Vastaranta, M., Holopainen, M. & Hyyppa, J. (2012). Prediction of plot-level forest variables using TerraSAR-X stereo SAR data. *Remote Sensing of Environment*, 117: 338-347.

Karyanto, O. (2011). *Personal communication* (November 13th, 2011).

Kasmujiono, M. (2011). *Personal communication* (November 25th, 2011).

Kindermann, G., Obersteiner, M., Sohngen, B., Sathaye, J., Andrasko, K., Rametsteiner, E., Schlamadinger, B., Wunder, S. & Beach, R. (2008). Global cost estimates of reducing carbon emissions through avoided deforestation. *Proceedings of the National Academy of Sciences of the United States of America*, 105 (30): 10302-10307.

McKibben, B. (2007). Climate change 2007: The physical science basis: Summary for policymakers. *New York Review of Books*, 54 (4): 44-45.

MDA. (2007). MacDonald, Dettwiler and Associates. Available at: http://gs.mdacorporation.com/SatelliteData/Radarsat2/Radarsat2.aspx (accessed: December 7th, 2012).

Neef, T., Dutra, L. V., dos Santos, J., o, R., Freitas, C. d. C. & Araujo, L. S. (2005). Tropical Forest Measurement by Interferometric Height Modeling and P-Band Radar Backscatter. *Forest Science*, 51 (6): 585-594.

NGA. (2012). *NGA EGM96 Geoid Calculator*. Available at: http://earth-info.nga.mil/GandG/wgs84/gravitymod/egm96/intpt.html (accessed: November 10th, 2011).

Perko, R., Raggam, H., Deutscher, J., Gutjahr, K. & Schardt, M. (2011). Forest Assessment Using High Resolution SAR Data in X-Band. *Remote Sensing*, 3 (4): 792-815.

R-project. (2012). Available at: http://www.r-project.org/ (accessed: December 13th, 2012).

Rosenqvist, Å., Milne, A., Lucas, R., Imhoff, M. & Dobson, C. (2003). A review of remote sensing technology in support of the Kyoto Protocol. *Environmental Science & Policy*, 6 (5): 441-455.

SAS. (2012). Available at: http://www.sas.com/ (accessed: December 13th, 2012).

Slade, B. (2011). *RADARSAT-2 Product description*: MacDonald, Dettwiler and Associates Ltd.

Solberg, S., Astrup, R., Bollandsas, O. M., Naesset, E. & Weydahl, D. J. (2010). Deriving forest monitoring variables from X-band InSAR SRTM height. *Canadian Journal of Remote Sensing*, 36 (1): 68-79.

TopCon. (2012). *HiPer II*. Available at: http://www.topconpositioning.com/products/gps/receivers/hiper-ii (accessed: December 7th, 2012).

Toutin, T. & Gray, L. (2000). State-of-the-art of elevation extraction from satellite SAR data. *ISPRS Journal of Photogrammetry and Remote Sensing*, 55 (1): 13-33.

Toutin, T. (2010). Impact of Radarsat-2 SAR Ultrafine-Mode Parameters on Stereo-Radargrammetric DEMs. *Geoscience and Remote Sensing, IEEE Transactions on*, 48 (10): 3816-3823.

Toutin, T. & Omari, K. (2011). A "New Hybrid" Modeling for Geometric Processing of Radarsat-2 data without User's GCP. *Photogrammetric Engineering and Remote Sensing*, 77 (6): 601-608.

Toutin, T. (2012). Radarsat-2 DSM Generation With New Hybrid, Deterministic, and Empirical Geometric Modeling Without GCP. *Ieee Transactions on Geoscience and Remote Sensing*, 50 (5): 2049-2055.

Wagner, W., Pathe, C., Doubkova, M., Sabel, D., Bartsch, A., Hasenauer, S., Blöschl, G., Scipal, K., Martínez-Fernández, J. & Löw, A. (2008). Temporal Stability of Soil Moisture and Radar Backscatter Observed by the Advanced Synthetic Aperture Radar (ASAR). *Sensors*, 8 (2): 1174-1197.

Weydahl, D. J. (2012). *Personal communication* (December 13th, 2012).